

Exact Meander Asymptotics: a Numerical Check

P. Di Francesco*,

E. Guitter#,

Service de Physique Théorique, C.E.A. Saclay,

F-91191 Gif sur Yvette, France

and

J. L. Jacobsen&

LPTMS, bâtiment 100, Université Paris-Sud,

F-91405 Orsay, France

Abstract: This note addresses the meander enumeration problem: “Count all topologically inequivalent configurations of a closed planar non self-intersecting curve crossing a line through a given number of points”. We review a description of meanders introduced recently in terms of the coupling to gravity of a two-flavored fully-packed loop model. The subsequent analytic predictions for various meandric configuration exponents are checked against exact enumeration, using a transfer matrix method, with an excellent agreement.

03/00

* e-mail:philippe@spht.saclay.cea.fr

e-mail:gutter@spht.saclay.cea.fr

& e-mail:jacobsen@ipno.in2p3.fr

1. Introduction

The meander problem is one of those tantalizing questions that has resisted a definite solution for decades, although it is very easy to state: “Given a positive integer n , in how many topologically distinct ways can a closed non-intersecting planar curve (*road*) cross a straight line (*river*) in exactly $2n$ points (*bridges*)?”

Originally an exercise of recreational mathematics [1], the meander problem turned out to have applications in the most various branches of science: Sorting algorithms in computer science [2], enumeration of ovals of planar algebraic curves [3], classification of three-manifolds [4], and in connection with a particular type of self-avoiding walk describing the compact folding of a linear chain [5].

An obvious strategy would of course be to evaluate the first few meander numbers M_n , in the hope of finding an explicit formula, valid for arbitrary n . Such enumerative approaches exist on various levels of sophistication [6-9], and a recent transfer matrix method [10] carried out this program up to $n = 24$. Although an explicit expression for M_n appears to be out of reach, it became clear that, in analogy with two-dimensional lattice polymers, the meander numbers scale asymptotically as $M_n \sim CR^{2n}/n^\alpha$, where R is a connectivity constant and α a configuration exponent.

A major achievement of random matrix theory has been to deal with precisely such asymptotic enumeration problems [11]. It is therefore natural to apply such techniques to the meander problem [12-14]. In particular it has emerged that a generalized multi-road multi-river meander problem, in which each closed segment of river (resp. road) is given the statistical weight n_1 (resp. n_2), can be cast as a Hermitian matrix model, known as the $O(n_1, n_2)$ model [5]. In the special case of $n_2 = 1$ this model is soluble by a saddle-point method, leading to an exact evaluation of R and α [15,16]. Unfortunately these results do not pertain to the original meander problem, which is recovered in the limit $n_1, n_2 \rightarrow 0$.

In a recent publication [17] it was argued that the meander problem is a particular realization of the coupling to gravity of a certain two-flavored loop model [18], initially defined on the square lattice. The most general gravitational version of this loop model is a generalization of the meander problem in which river and road segments, counted with their respective weights of n_1 and n_2 , are allowed to cross as well as to touch one another without crossing (tangency points) [17]. We shall refer to this model as *tangent meanders*. On the regular lattice, directed segments of river and road can be inserted by means of certain magnetic defect operators, for which the anomalous dimensions are known exactly.

When dressed by quantum gravity, these dimensions transform according to the KPZ formula [19]. This transformation allows one to extract *exact* values for the configuration exponent α of tangent meanders, whereas R , being a non-universal quantity, is lost in the process. The connection to the original meander problem is then made by arguing that tangency is *irrelevant* from a renormalization point of view [17]. Thus, the result for α in fact pertains to the original meander problem, i.e. to the gravitational $O(n_1, n_2)$ model. Moreover, the operator content of the theory gives access to other geometries, involving several rivers, possibly with marked points, as well as semi-meanders (river with a source).

Here we review and extend the arguments of [17]. In particular we establish the irrelevance of tangency rigorously in a number of special cases. We also add credibility to the theoretical predictions by performing extensive exact enumerations of various meander geometries, using a generalization of the transfer matrix method presented in [10]. We first address multi-component meanders, that allow for precisely checking the predicted value of the central charge of the underlying conformal theory. Next we explore two distinct river geometries, namely (i) two parallel rivers, and (ii) one semi-infinite river, that permit to validate their magnetic operator formulation within the corresponding conformal theory. We finally consider the case of tangent meanders and verify the irrelevance of tangency, thus confirming the cornerstone of the argument. In all cases we find an excellent agreement with theory, typically confirming the configuration exponents with 4–5 significant digits.

The paper is organized as follows. In Section 2 we review the square-lattice loop model and its solution, before presenting its gravitationally dressed version and the results for the asymptotics of a range of meander-related quantities. The transfer matrix algorithms are presented in Section 3, and in Section 4 we analyze the data and compare them to the theoretical predictions. Our conclusions and some perspectives can be found in Section 5.

2. Theory: from fully-packed loop gases to meanders

In this Section, we review the arguments of Ref. [17] relating the meander problem to the gravitational version of a particular fully-packed loop model initially defined on the square lattice [18]. The effect of gravity is to replace the lattice with a random quadrangulation of the sphere. The lattice loop gas is described in subsection 2.1 while its conformal structure is presented in subsection 2.2. The connection to meanders via two-dimensional quantum gravity is explained in subsection 2.3. This leads naturally to an effective field theory description detailed in subsection 2.4 together with the subsequent predictions for various meandric configuration exponents.

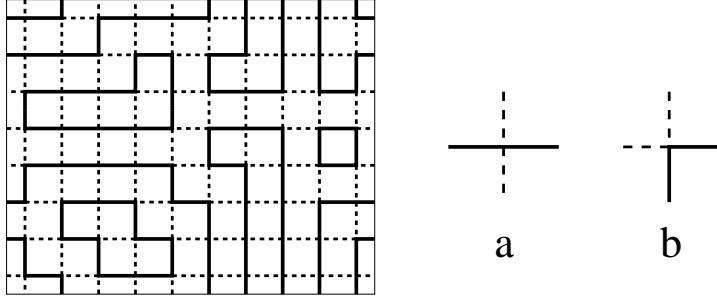


Fig. 1: A typical fully-packed loop configuration on the square lattice. Assuming doubly periodic boundary conditions, there are 6 black loops (solid lines) and 4 white ones (dashed lines). Up to rotations, the vertices of the model are of the two types (a) “crossing” or (b) “avoiding”.

2.1. Fully-packed loop gas on the square lattice

The configurations of the fully-packed loop model that we shall consider are defined by assigning to each edge of the two-dimensional square lattice either of two colors (say, black or white, represented as solid or dashed lines in Fig. 1, also referred to as 1 and 2 in the following) in such a way that each vertex has exactly two black and two white incident edges. Up to obvious rotations, this gives rise to the two vertex configurations depicted in Fig. 1 in which the black and white lines either avoid or cross each other. Note that with periodic boundary conditions the black and white lines form loops. It is interesting to remark that the fully-packed loop model’s configurations defined here differ from those of the so-called densely packed loop model [18] in that each vertex is visited by a black *and* a white loop, whereas in the dense case, loops of a given (say black) color are not constrained to visit all vertices.

The partition function of the fully-packed loop model is then defined by assigning a weight n_1 per black loop and n_2 per white one,

$$Z_{\text{FPL}}(n_1, n_2) = \sum_{\text{fully-packed loop configurations}} n_1^{L_1} n_2^{L_2} , \quad (2.1)$$

where we have denoted by L_i the total numbers of loops of each color $i = 1, 2$. Following [18] we shall denote the model with partition function (2.1) as the $\text{FPL}^2(n_1, n_2)$ model, while the densely packed version is referred to as the $\text{DPL}^2(n_1, n_2)$ model.

The loop weights n_i may be recast as local Boltzmann weights as follows. This step is important in the field theoretic description of the model, since it leads to a *local* field theory. Let us assign to each black or white loop an arbitrary orientation, and attach to

each vertex a local Boltzmann weight $e^{i\pi(\epsilon_1 e_1 + \epsilon_2 e_2)/4}$ where $\epsilon_i = 1$ if the oriented loop of color i makes a left turn, $\epsilon_i = 0$ if it goes straight, and $\epsilon_i = -1$ if it makes a right turn. Summing over all possible orientations of all loops, we get a factor $2 \cos \pi e_i$ per loop of color i , and therefore we reproduce the desired loop weights by setting

$$n_1 = 2 \cos \pi e_1, \quad n_2 = 2 \cos \pi e_2. \quad (2.2)$$

2.2. Conformal field theory description

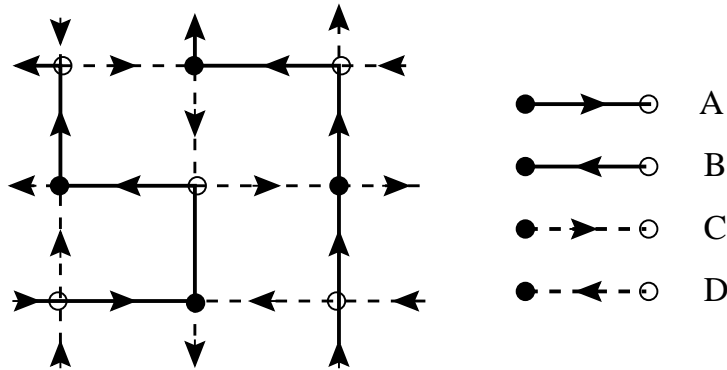


Fig. 2: A typical configuration of the FPL^2 model together with the bicoloration of its vertices (checkerboard of filled (●) and empty (○) dots). We have added the corresponding dictionary that allows to map the loop configurations onto A, B, C, D labelings of the edges.

The $FPL^2(n_1, n_2)$ model is known to be critical for $0 \leq n_i \leq 2$ [18], and is described in the continuum limit by a simple conformal field theory based on free scalar fields. To identify its basic degrees of freedom, it is useful to rephrase the model as a (three-dimensional) height model as follows. Starting from an oriented fully-packed black and white loop configuration, we first bicolor the vertices of the square lattice, say with alternating filled (●) and empty (○) dots. Then we use the dictionary of Fig. 2 to assign one of the four labels A, B, C, D to each colored and oriented edge. With this convention, it is clear that edges of type $ABAB \dots$ alternate along black loops, whereas edges of type $CD CD \dots$ alternate along white loops, and that each vertex has one incident edge of each type A, B, C and D . It is seen that the four-labeling with A, B, C, D is in one-to-one correspondence with the coloring *and* orientation of edges of the FPL^2 model. In particular, the orientation of

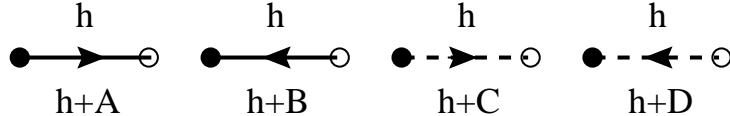


Fig. 3: Rules determining the change of the height variable across labeled edges. We adopt the Ampère convention that the height is increased (resp. decreased) by the edge value if the arrow of the edge points to the left (resp. right). The edge labels must be interpreted as three-dimensional vectors with the respective values \mathbf{A} , $-\mathbf{B}$, \mathbf{C} , $-\mathbf{D}$.

a given black or white loop is reversed if we interchange the A and B or C and D labels along the loop.

The above colors allow for the definition of a dual vector height variable on the center of each face of the lattice. Indeed, viewing as vectors the A, B, C, D labeling of the edges of the lattice, let us arbitrarily fix the height to be zero on a given face of the lattice, and define it on all other faces by successive use the rules of Fig. 3 for the transition from a face to any of its neighbors. Note that it is necessary to impose the condition $\mathbf{A} + \mathbf{B} + \mathbf{C} + \mathbf{D} = 0$ to ensure that the heights are consistently defined around each vertex. We may therefore assume in all generality that $\mathbf{A}, \mathbf{B}, \mathbf{C}, \mathbf{D}$ are actually four vectors in \mathbb{R}^3 with vanishing sum. To get a more symmetric formulation, we may further fix $\mathbf{A}, \mathbf{B}, \mathbf{C}, \mathbf{D}$ to be the four unit vectors pointing from the center of a tetrahedron towards its vertices. The heights are then clearly three-dimensional, as linear combinations of $\mathbf{A}, \mathbf{B}, \mathbf{C}, \mathbf{D}$. In the continuum limit, it was argued [18] that the three-dimensional height variable turns into a three-dimensional scalar field. Moreover the symmetries of the model completely fix the action for these fields and the corresponding field theory is conformal, with central charge

$$c_{\text{FPL}}(n_1, n_2) = 3 - 6 \left(\frac{e_1^2}{1 - e_1} + \frac{e_2^2}{1 - e_2} \right), \quad (2.3)$$

where e_i have been defined in (2.2) and are constrained by $0 \leq e_i \leq 1/2$. Actually the shift in the central charge away from 3 is due to the introduction of a background electric charge, ensuring that loops that have non-trivial winding with respect to the periodic boundary conditions still get correctly weighted, although for such loops the argument given before (2.2) no longer holds true.

2.3. Meanders: the coupling to gravity

To finally get to meanders, we must consider the coupling of the $\text{FPL}^2(n_1, n_2)$ model to two-dimensional quantum gravity, by allowing the square lattice to fluctuate into arbitrary

planar four-valent graphs. For each such graph the fully-packed loop model is still defined by coloring the edges black or white and allowing only the vertices shown in Fig. 1. As before, each colored loop is weighted by the appropriate n_i factor ($i = 1, 2$).

If we try to go through the steps of the previous section, namely by transforming the model into a height model, the issue of bicolorability of the vertices of the lattice becomes crucial on a random four-valent graph. Indeed, not all such graphs are vertex-bicolorable. So the coupling to gravity *stricto sensu* (sum over arbitrary planar four-valent graphs) will destroy this property.

We may now follow either of the two following paths. First, we can repair this and *impose* that the particular coupling to gravity preserve the bicolorability, namely that the gravitational model be defined on the set of vertex-bicolorable four-valent graphs only. These graphs are dual to the so-called Eulerian quadrangulations. In genus zero (planar case), the latter are characterized by the fact that all their vertices have an even valency (Euler condition). If we couple the $\text{FPL}^2(n_1, n_2)$ model to Eulerian gravity, the A, B, C, D labeling is still well-defined, as well as the three-dimensional height, now defined on the centers of the faces of the graph. This preserves the degrees of freedom of the flat space model entirely in the gravitational formulation. This approach was initiated in [20] for the simpler case of the fully packed $O(n)$ model with only one type of loops.

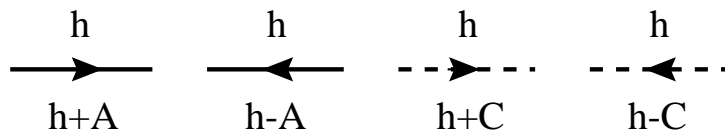


Fig. 4: Rules determining the change of the height variable across labeled edges in the non-bicolored case. These rules are identical to those of Fig. 3, with the further restriction that $\mathbf{B} = -\mathbf{A}$ and $\mathbf{D} = -\mathbf{C}$, allowing to ignore the bicoloration of vertices.

On the other hand, we can study how the degrees of freedom of the model are affected by the coupling to ordinary (non-Eulerian) quantum gravity. Having lost the bicolorability of vertices, it is no longer possible to distinguish between A and B labels on one hand, and C and D on the other. We may still define an edge-labeling of the graph in one-to-one correspondence with oriented colored fully-packed loop configurations on the graph, but with vectors $\mathbf{A}, \mathbf{B}, \mathbf{C}, \mathbf{D}$ satisfying the two constraints $\mathbf{A} + \mathbf{B} = 0$ and $\mathbf{C} + \mathbf{D} = 0$, and picking \mathbf{A} and \mathbf{C} to be two perpendicular unit vectors in \mathbb{R}^2 . The correspondence between color/orientation and A, C labels reads as in Fig. 4. As in Eq. (2.1), the model is further

completed by attaching weights n_i to each loop of color $i = 1, 2$. We may now define a height variable on the centers of the faces of the graph, by use of the previous rules. The main difference is that the height now lives in two dimensions (the plane generated by **A** and **C**). Such a dimensional reduction is also observed on the square lattice when going from the $\text{FPL}^2(n_1, n_2)$ to the $\text{DPL}^2(n_1, n_2)$ model [18]; interestingly enough, the same dimensional reduction is also observed when the FPL^2 model is defined on the Manhattan square lattice, with oriented loops respecting the Manhattan orientation [21]. It results in a shift $c \rightarrow c - 1$ in the central charge of the underlying conformal theory, namely

$$c(n_1, n_2) = c_{\text{DPL}}(n_1, n_2) \equiv 2 - 6 \left(\frac{e_1^2}{1 - e_1} + \frac{e_2^2}{1 - e_2} \right). \quad (2.4)$$

In the following, we will concentrate on this formulation, eventually leading to the solution of the meander problem.

The partition function of the fully-packed model coupled to *ordinary* quantum gravity, hereafter referred to as the $\text{GFPL}^2(n_1, n_2)$ model, reads in genus zero:

$$Z_{\text{GFPL}}(n_1, n_2; x, y) = \sum_{\substack{\text{four-valent} \\ \text{graphs } \Gamma}} \sum_{\substack{\text{planar FPL} \\ \text{configs. } \mathbf{C} \\ \text{on } \Gamma}} \frac{1}{|\text{Aut}(\Gamma, \mathbf{C})|} n_1^{L_1} n_2^{L_2} x^{V_a(\Gamma)} y^{V_b(\Gamma)}, \quad (2.5)$$

where the sum extends over all the genus zero four-valent graphs Γ , and $|\text{Aut}(\Gamma, \mathbf{C})|$ is the order of the symmetry group of Γ equipped with the loop configuration \mathbf{C} . We have also denoted by V_a, V_b the total numbers of vertices of type a and b defined in Fig. 1 in the particular loop configuration, namely we have weighted each crossing of a black and a white loop by x and each avoiding by y . When $x = y$, these are interpreted as the cosmological constant, as the total number of vertices $V_a + V_b$ of Γ is also the area of the corresponding dual random surface.

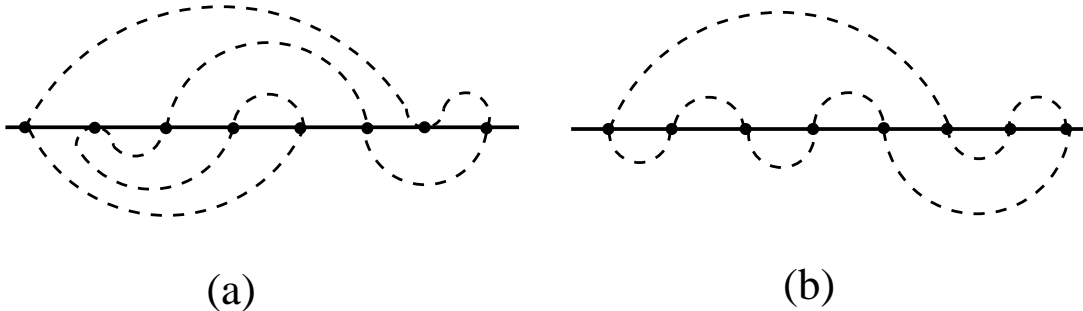


Fig. 5: Examples of (a) a tangent meander with 2 tangency points (b-vertices) and 6 bridges (a-vertices) and (b) a meander with 8 bridges.

To generate meanders, we must now extract from (2.5) the configurations with only one black and one white loop, that will respectively play the role of the river and the road. This is done by taking the limit $n_1, n_2 \rightarrow 0$ in (2.5), resulting in

$$\begin{aligned} Z_{\text{GFPL}}(x, y) &= \lim_{n_1, n_2 \rightarrow 0} \frac{1}{n_1 n_2} (Z_{\text{GFPL}}(n_1, n_2; x, y) - 1) \\ &= \sum_{\substack{n, p \geq 0 \\ n+p \geq 1}} \frac{x^{2n} y^p}{2(2n+p)} \mu_{2n, p}, \end{aligned} \quad (2.6)$$

where we have denoted by $\mu_{2n, p}$ the total number of *tangent meanders* with $2n$ crossings and p tangency points, i.e. configurations of a non-selfintersecting circuit (road) crossing a line (river) through $2n$ points (bridges) and touching the river p times (tangent contacts), as illustrated in Fig. 5. The usual meander numbers defined in [5] correspond to only crossings and no tangency points and read $M_n = \mu_{2n, 0}$. In (2.6), the prefactor $1/(2(2n+p))$ stands for the symmetry factor attached to the tangent meanders: going from the graph to the representation where the river is a line, we may indeed cut the river loop in $2n+p$ places in between bridges and tangency points, and we still have 2 choices for the up/down position.

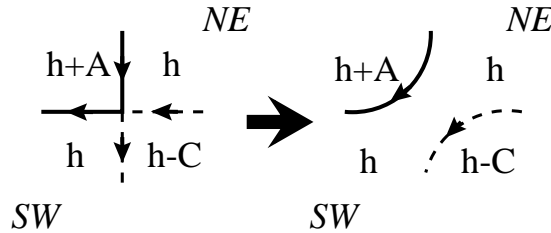


Fig. 6: A type b vertex of the FPL^2 gravitational model, together with its dual height configuration. We note that the NE and SW heights are identical. We may therefore undo the vertex as shown, which results in its irrelevance.

The meanders are therefore generated by the function (2.6) for $y = 0$. Let us now show that the universality class of the tangent meanders is the same as that of meanders. In the transformation into a (two-dimensional) height model, the “tangency” vertex b of Fig. 1 corresponds to the arrangements of heights on adjacent faces depicted in Fig. 6. We notice that the NE and SW heights are identical, irrespectively of the orientations of the two loops. This means that as far as the height variable is concerned this vertex may be simply removed as shown. We conclude that the b-vertex of the model is irrelevant [17]. As

a consequence, we expect the following asymptotics for $N = 2n + p$ large of the partition function $\mu_N(x, y)$ for tangent meanders with a total N of bridges and tangency points:

$$\mu_N(x, y) = \sum_{\substack{n, p \geq 0 \\ 2n+p=N}} x^{2n} y^p \mu_{2n, p} \sim C(x, y) \frac{R(x, y)^N}{N^\alpha}, \quad (2.7)$$

where the configuration exponent α is independent of x and y for $x > 0$ and $y \geq 0$. In particular, when $y = 0$, α is identified with the meander configuration exponent $M_n \sim cR^n/n^\alpha$. The irrelevance of the vertex b will be checked numerically in subsection 4.4 below.

More generally, we may consider tangent meanders with one single river, but arbitrarily many possibly interlocking closed roads. This is given by the $n_1 \rightarrow 0$ limit of (2.5) while $n_2 = q$ is kept finite, namely

$$\begin{aligned} Z_{\text{GFPL}}(q; x, y) &= \lim_{n_1 \rightarrow 0} \frac{1}{n_1} (Z_{\text{GFPL}}(n_1, n_2 = q; x, y) - 1) \\ &= \sum_{n, p \geq 0; n+p \geq 1} \frac{x^{2n} y^p}{2(2n+p)} \mu_{2n, p}(q), \end{aligned} \quad (2.8)$$

where we have defined the tangent meander polynomial

$$\mu_{2n, p}(q) = \sum_{k=1}^{n+p} \mu_{2n, p}^{(k)} q^k \quad (2.9)$$

with coefficients $\mu_{2n, p}^{(k)}$ being the numbers of tangent meanders with k connected components of road, $2n$ bridges and p tangency points. The polynomial $\mu_{2n, 0}(q) = m_n(q)$ coincides with the meander polynomial defined in [5]. We may also define the canonical partition function:

$$\mu_N(q; x, y) = \sum_{\substack{n, p \geq 0 \\ 2n+p=N}} x^{2n} y^p \mu_{2n, p}(q). \quad (2.10)$$

We expect a large N asymptotic behavior of the form

$$\mu_N(q; x, y) \sim C(q; x, y) \frac{R(q; x, y)^N}{N^{\alpha(q)}}, \quad (2.11)$$

where the configuration exponent $\alpha(q)$ only depends on q and not on y/x , due to the irrelevance of the b -vertex. In particular, it takes the same value at $y/x = 0$, where it coincides with the multi-component meander configuration exponent, i.e. $m_n(q) \sim C(q)R(q)^{2n}/n^{\alpha(q)}$.

In the special case $q = 1$ of arbitrarily many roads without extra weight, these numbers can be computed exactly. Indeed, we may decompose an arbitrary multi-component tangent meander with $2n$ bridges and p tangency points into its upper part (above the river) and lower part (below), and consider that these may be obtained first by picking p_1 points among the total $N = 2n + p$ to be the upper tangency points, and $p_2 = p - p_1$ to be the lower ones. Let us then draw small semi-circles tangent to the p points, p_1 of them in the upper half, p_2 in the lower. With the $2n$ bridges, we have now a total of $2n + 2p_1$ points in the upper half and $2n + 2p_2$ in the lower one to be connected among themselves by pairs through non-intersecting arches. Such upper and lower arch configurations have already been extensively studied in [5]. In particular, there are $c_m = (2m)!/(m!(m+1)!)$ (c_m are the Catalan numbers) distinct upper arch configurations connecting $2m$ bridges by pairs in the upper half plane above the river. Hence we must choose among the c_{n+p_1} upper arch configurations and the c_{n+p_2} lower ones to form an arbitrary multi-component tangent meander. This results in the formula

$$\mu_{2n,p}(q=1) = \sum_{p_1=0}^p \frac{(2n+p)!}{p_1!(p-p_1)!(2n)!} c_{n+p_1} c_{n+p-p_1}, \quad (2.12)$$

where the combinatorial factor accounts for the choices of upper and lower tangent points among the total of $2n + p$. The corresponding partition function (2.10) reads

$$\mu_N(q=1; x, y) = N! \sum_{\substack{n,p \\ 2n+p=N}} \frac{x^{2n}}{(2n)!} \sum_{\substack{p_1, p_2 \\ p_1+p_2=p}} \frac{y^{p_1}}{p_1!} \frac{y^{p_2}}{p_2!} c_{n+p_1} c_{n+p_2}. \quad (2.13)$$

When N is large, this is easily estimated by a saddle-point technique, making use of the Stirling formula. For $x, y \geq 0$, we find the large N behavior

$$\mu_N(q=1; x, y) \sim \frac{(4x + 8y)^N}{N^3} \quad (2.14)$$

up to a multiplicative constant depending on x and y only. This shows explicitly that the exponent $\alpha(q=1) = 3$ is robust and is not affected by the respective values of x and y . This confirms in particular the above-mentioned irrelevance of the b-vertex, as α keeps to the same value, irrespectively of y .

In conclusion, the meander numbers belong to the universality class of the GFPL²(n_1, n_2) model at $n_1, n_2 \rightarrow 0$. The corresponding flat space theory has the central charge (2.4) with, according to (2.2), $e_1 = e_2 = 1/2$, hence $c = -4$. In the next subsection, we will concentrate on the partition function $Z_{\text{GFPL}}(x, y = 0)$ (2.6) that generates the meander numbers.

More generally, the multi-component meander polynomial belongs to the universality class of the $\text{GFPL}^2(n_1, n_2)$ model, with $n_1 \rightarrow 0$ and $n_2 = q$ and central charge (2.4). Finally, we may also consider meanders with arbitrarily many rivers and roads, with a weight n_1 per river and n_2 per road; these objects belong to the universality class of the $\text{GFPL}^2(n_1, n_2)$ model. It has been shown using matrix model techniques that the $\text{GFPL}^2(n_1 = 1, n_2 = q)$ with $y = 0$ belongs to the same universality class as the $\text{O}(q)$ model when coupled to ordinary gravity (i.e. defined on arbitrary four-valent graphs) [15]. More precisely, the number of multi-river, multi-road meanders with a total of $2n$ intersections and with a weight q per road and 1 per river, also weighted by their inverse symmetry factor (and multiplied by $4n$ to make it comparable to M_n) behaves for large n as

$$C(1, q)R(1, q)^{2n}/n^{\alpha(1, q)}, \quad R(1, q) = 2\frac{\sin^2(\pi e/2)}{e^2}, \quad (2.15)$$

$$\alpha(1, q) = \frac{2 - e}{1 - e}, \quad q = 2 \cos(\pi e).$$

The determination of $R(1, q)$ on which we have no prediction was made possible by an explicit mapping of the matrix model onto a particular version of the gravitational $\text{O}(q)$ model, where the critical value of the cosmological constant x_c can be explicitly calculated. The value $\alpha(1, q)$ corresponds to the expected scaling behavior of a $c = 1 - 6e^2/(1 - e)$ (c.f. (2.4) with $n_1 = 1$ and $n_2 = q$) conformal theory coupled to two-dimensional quantum gravity. In particular, when $q = 1$, $c = 0$ we get $\alpha(1, 1) = 5/2$ as expected in “pure gravity” without matter.

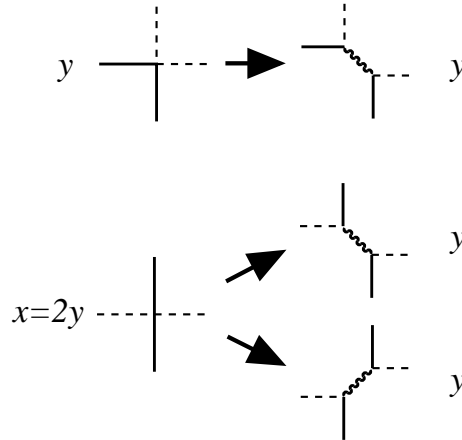


Fig. 7: The transformation of the four-valent a- and b-vertices of the FPL^2 model into pairs of trivalent ones connected by an extra (gray) edge, depicted as a wavy line. Due to the 1 to 2 correspondence in the case of the a-vertex, we must restrict ourselves to the case $x = 2y$, and then each trivalent vertex receives a weight \sqrt{y} .

It is interesting to notice that if we restore the b-vertex (with a weight y per vertex), and choose specifically $x = 2y$, then the GFPL²(1, q) model can be mapped onto that of tricoloring the edges of a random trivalent graph (with black, gray and white edge colors) with a weight q per loop of alternating say gray and white colors. Indeed, the quartic vertices a and b may be decomposed into pairs of connected trivalent ones as shown in Fig. 7 in which we have added a third type of edge, say with gray color. This transformation allows to map the configurations of the GFPL²(1, q) model weighted by $x = 2y$ per a-vertex and y per b-vertex onto those of arbitrary edge-tricolored trivalent graphs, with a weight \sqrt{y} per vertex and q per white/gray loop. The latter model was solved in [22] and identified with a particular version of the fully-packed O($2q$) model on random trivalent graphs: indeed, the white and gray edges form naturally fully packed loops on the graph, and on each loop we may interchange the two colors to generate new tricolorings, hence we may simply draw fully-packed loops on trivalent graphs, and attach a weight $2q$ to each of these loops. But the loops have all even lengths and this turns out to dimensionally reduce the model to an effective O($2q/2 = q$) one with central charge $c = 1 - 6e^2/(1 - e)$ as before. This particular point therefore lies in the same universality class as the model without b-vertex, which gives another explicit example of the irrelevance of the b-vertex.

2.4. Field theory description of meandric numbers

The coupling of a conformal field theory with central charge $c \leq 1$ to two-dimensional quantum gravity (i.e. its definition on random surfaces) has a simple field-theoretical formulation in terms of the Liouville field describing the conformal classes of metrics of the surfaces. This has led to a number of results, including the precise determination of various critical exponents. Indeed, the gravitational theory (say on genus zero surfaces) displays a critical behavior as a function of the cosmological constant x . In particular, there exists a finite value x_c of x at which the (connected) partition function behaves as

$$Z(x) \sim (x_c - x)^{2-\gamma(c)}, \quad (2.16)$$

where the string susceptibility exponent γ is related to the central charge c through [19]

$$\gamma(c) = \frac{c - 1 - \sqrt{(1 - c)(25 - c)}}{12}. \quad (2.17)$$

When applied to the $\text{DPL}^2(0,0)$ model of the previous section (with $c = -4$), whose gravitational version was shown to describe meanders, we find that

$$\gamma \equiv \gamma(-4) = -\frac{5 + \sqrt{145}}{12}. \quad (2.18)$$

Comparing (2.16) with the expansion

$$Z_{\text{GFPL}}(x) = \sum_{n \geq 1} \frac{x^{2n}}{4n} M_n \quad (2.19)$$

we deduce the asymptotic behavior [17]

$$M_n \sim C \frac{x_c^{-2n}}{n^\alpha}, \quad \alpha = 2 - \gamma = \frac{29 + \sqrt{145}}{12}. \quad (2.20)$$

Moreover, a number of the operators of the flat space conformal theory (in particular the spinless ones, with conformal dimensions $h = \bar{h}$) get dressed by gravity, in such a way that they acquire anomalous scaling dimensions. Any given operator ϕ_k with dimensions $h_k = \bar{h}_k$, is dressed into an operator $\tilde{\phi}_k$ with dressed dimension Δ_k such that the correlation functions behave as

$$\langle \tilde{\phi}_{k_1} \tilde{\phi}_{k_2} \dots \tilde{\phi}_{k_p} \rangle \sim (x_c - x)^{2 - \gamma + \Sigma(\Delta_{k_i} - 1)} \quad (2.21)$$

when x approaches the critical value x_c , and where the dressed dimension Δ_k is related to the flat space conformal dimension h_k through

$$\Delta_k = \frac{\sqrt{1 - c + 24h_k} - \sqrt{1 - c}}{\sqrt{25 - c} - \sqrt{1 - c}}. \quad (2.22)$$

Let us now present the operator content of the $c = -4$ conformal theory describing the dense loop model $\text{DPL}^2(0,0)$ [18]. For generic values of n_1, n_2 , the $\text{DPL}^2(n_1, n_2)$ has a continuum description as a two-component scalar field with charges at infinity. More precisely, it is a Coulomb gas made of two decoupled scalar fields, with $c = c(n_i) = 1 - 6e_i^2/(1 - e_i) = -2$ at $n_i = 0$ ($e_i = 1/2$) respectively, each viewed as the effective field theory of loops of one color. In particular, within each scalar field theory (indexed by the color $i = 1, 2$), there exist operators $\psi_k^{(i)}(z)$ that create k oriented defect lines (of color i) for the scalar field, with conformal dimensions [23]:

$$h_k^{(i)} = \frac{k^2 - 4}{32} \quad (2.23)$$

at $n_i = 0$. In the Coulomb gas formalism, these correspond to electromagnetic operators with electric charge e_i (spin-wave) and magnetic charge $\pm k/2$ (vortex), according to whether the defect line is oriented from or to the insertion point, and k is a strictly positive integer. The electric charge ensures that, if the defect lines wind around the insertion point, all extra curvature weights get cancelled [24]. For $k = 0$, (2.23) must be replaced by $h_0^{(i)} = 0$ corresponding to the identity operator. The correlation functions must have a vanishing total magnetic charge. Although these operators also carry an electric charge $1/2 = e_1 = e_2$, the electric neutrality of correlators imposes no extra condition¹.

We may also combine operators for both colors, namely consider mixed operators $\psi_{k_1, k_2} = \psi_{k_1}^{(1)} \psi_{k_2}^{(2)}$ with conformal dimension $h_{k_1, k_2} = h_{k_1}^{(1)} + h_{k_2}^{(2)}$ for $k_1, k_2 \in \mathbb{Z}$.

Let us now study the dressing of these operators by gravity, and interpret them in meandric terms. The dressed operator $\tilde{\psi}_k^{(i)}$ again corresponds to the creation of a vertex with $|k|$ outgoing ($k > 0$) or incoming ($k < 0$) lines of color i .

As a first example, note that $h_2^{(i)} = 0$. From the formula (2.21), it is clear that the operators $\tilde{\psi}_{\pm 2}^{(i)}$ have the effect of *marking* a point on a loop of color i . However, due to the constraint of global magnetic neutrality of correlators, the marking is not arbitrary as the loop of color i must have an even number of marks (alternating $\tilde{\psi}_2^{(i)}$ and $\tilde{\psi}_{-2}^{(i)}$). In particular, the one-point function $\langle \tilde{\psi}_2^{(1)} \rangle$ that would naively count meanders with a marked river turns out to vanish, while for instance the two-point function $\langle \tilde{\psi}_2^{(1)} \tilde{\psi}_{-2}^{(1)} \rangle$ indeed counts meanders with two marked points on the river. We will meet more examples of this below.

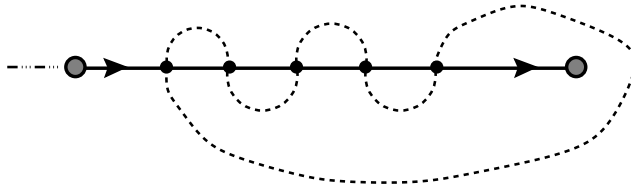


Fig. 8: A typical semi-meander configuration.

¹ It can be shown [25] that the corresponding non-minimal conformal theory pertaining to the loops of color i (with central charge $c = 1 - 6e_i^2/(1 - e_i)$) is equally well defined as a theory with central charge $c = 1$, in which the operator content has been reorganized, and in particular all of the above electromagnetic operators get a vanishing electric charge, while their magnetic one is unchanged. A supersymmetric version of this theory was also introduced in [26], in which arbitrary correlators could be calculated, irrespectively of the electric charge.

The first application of the above concerns the two point function describing the insertion of a segment of river (color 1)

$$\langle \tilde{\psi}_1^{(1)} \tilde{\psi}_{-1}^{(1)} \rangle \sim (x_c - x)^{2\Delta_1 - \gamma}. \quad (2.24)$$

Recall that when we take the limit $n_1, n_2 \rightarrow 0$, only diagrams with one connected component of river and one of road are selected. In the case of (2.24), the river forms a segment, around which the road can freely wind (see Fig. 8). To fix ambiguities, let us send one end of the river to infinity (say to the left) and therefore represent the river as a half-line (this is allowed as we work on Riemann sphere). The number of configurations of a closed road crossing a half-line (river with a source) through n bridges is defined as the semi-meander number \bar{M}_n . We immediately identify the series expansion of (2.24) as a function of x to be

$$\langle \tilde{\psi}_1^{(1)} \tilde{\psi}_{-1}^{(1)} \rangle = \sum_{n \geq 1} \bar{M}_n x^n. \quad (2.25)$$

We therefore deduce the semi-meander asymptotics [17]

$$\bar{M}_n \sim \bar{c} \frac{x_c^{-n}}{n^{\bar{\alpha}}} \quad \bar{\alpha} = 1 + 2\Delta_1 - \gamma = 1 + \frac{\sqrt{11}}{24}(\sqrt{5} + \sqrt{29}). \quad (2.26)$$

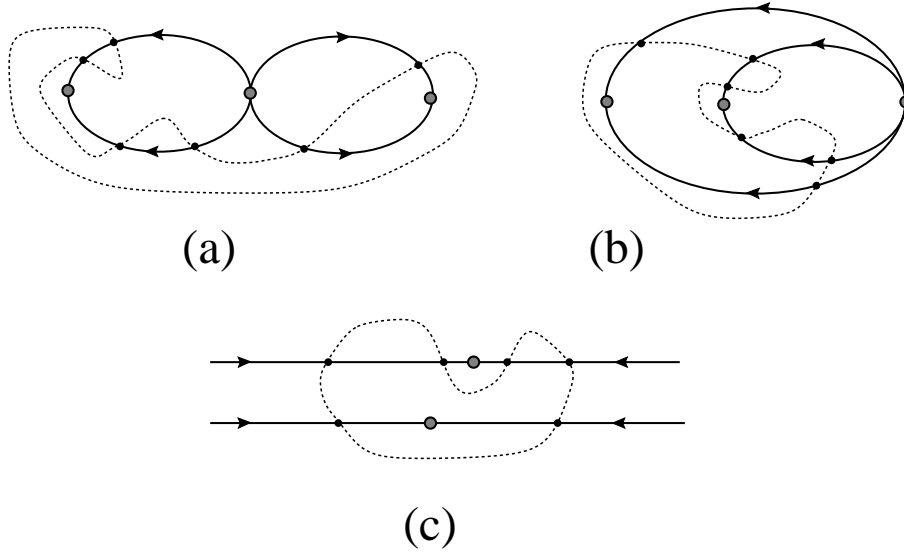


Fig. 9: A typical example of an eight figure river geometry (a). On the sphere, it is equivalent to the situation of (b), where the river crossing has been cleared of all winding pieces of road. This crossing may finally be sent to infinity (c) so as to form two parallel rivers. We have represented a particular configuration of road with $2p_1 = 4$ bridges on one loop and $2p_2 = 2$ on the other. Due to magnetic neutrality in the operator formulation, the two loops are marked as shown.

Our second example is the “eight” meander, in which the river forms the figure “eight”. To generate it, we need to insert an operator $\tilde{\psi}_4^{(1)}$, but magnetic neutrality forces us to insert two river-marking operators $\tilde{\psi}_{-2}^{(1)}$, one on each loop of the eight. The three-point correlation function $\langle \tilde{\psi}_4^{(1)}(\tilde{\psi}_{-2}^{(1)})^2 \rangle$ therefore generates the numbers of meanders whose river forms an eight figure, and with one marked point on each loop (see Fig. 9 (a)). To fix ambiguities, let us send the river-crossing to infinity. We may now represent the river as two parallel lines (all connected to the four-valent point at infinity), but the markings are still there (c.f. Fig. 9 (c)). Hence we have

$$\begin{aligned} \langle \tilde{\psi}_4^{(1)}(\tilde{\psi}_{-2}^{(1)})^2 \rangle &= \frac{1}{2} \sum_{n \geq 1} x^{2n} M_n^{2-\text{mark}} \\ &= \frac{1}{2} \sum_{n \geq 1} x^{2n} \sum_{p_1+p_2=n} (2p_1+1)(2p_2+1)M_{p_1,p_2}, \end{aligned} \quad (2.27)$$

where $M_n^{2-\text{mark}}$ is the number of meanders with two rivers, each of which is marked, and M_{p_1,p_2} is the number of meanders with two parallel rivers, and with $2p_1$ bridges on the first and $2p_2$ on the second (there are indeed $2p_i+1$ possible markings on a river loop with $2p_i$ bridges). Note the prefactor of $1/2$ accounting for the fact that we distinguish the top and bottom of the figure when we represent a two-river meander. From (2.21), we find that [17]

$$\begin{aligned} M_n^{2-\text{mark}} &\sim \text{const.} \frac{x_c^{-2n}}{n^{\alpha_{2-\text{mark}}}}, \\ \alpha_{2-\text{mark}} &= \Delta_4 + 2\Delta_2 - \gamma = \frac{1}{24}(\sqrt{5} + \sqrt{14})(\sqrt{5} + \sqrt{29}). \end{aligned} \quad (2.28)$$

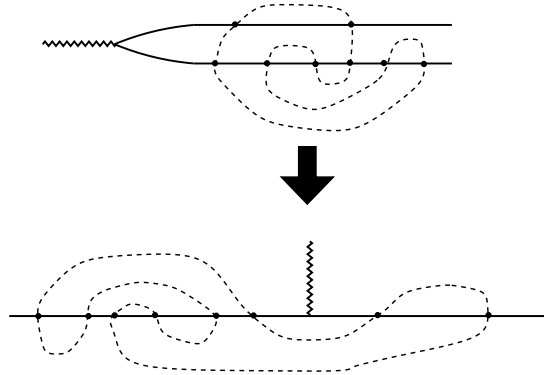


Fig. 10: A meander with two parallel rivers may be viewed as a meander “with a seam”. The point where the seam is attached is a remnant of the point at infinity (say to the left), where the two rivers meet. The seam just prevents roads from encircling this point.

It is also easy to determine the large n behavior of the unmarked meanders with two parallel rivers. Let us draw the two rivers horizontally. We may view the two rivers as connected to each other at their far left (at infinity) and represent them as in Fig. 10 as one marked line, such that a seam originates from the marked point that prevents any road from encircling the point to the left. So we have mapped two-river meanders onto one-river meanders with a seam. We may now generate all meanders with a seam by considering all the ways of placing a seam on the upper-half of meanders. If $E(M)$ denotes the total number of upper exterior arches of a meander M (namely arches that have no other arch above them), then there are $E(M) + 1$ distinct ways of decorating the meander with a seam. Hence the total number of two-river meanders reads

$$M_n^{2\text{-riv.}} = \sum_{\substack{\text{meanders } M \\ \text{with } 2n \text{ bridges}}} (E(M) + 1) = \langle E + 1 \rangle_n M_n, \quad (2.29)$$

where $\langle \dots \rangle_n$ stands for the average over all meanders with $2n$ bridges.

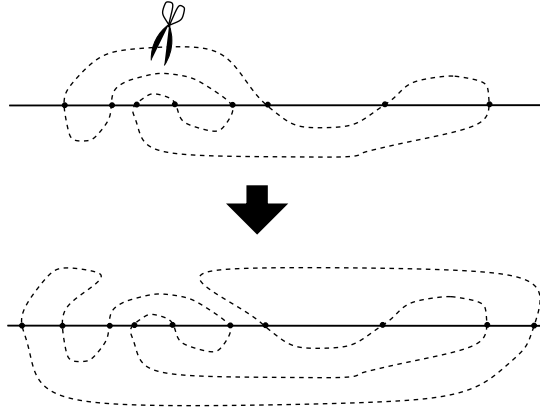


Fig. 11: How to construct a new meander with $2n + 2$ bridges from a meander with $2n$ bridges and one distinguished exterior arch, here on the upper half of the meander. We cut the corresponding arch, and glue it back across the river, by encircling the whole lower part of the meander. This is easily inverted within the set of meanders with $2n + 2$ bridges and one unique upper or lower exterior arch, showing that this construction gives only rise to distinct meanders.

We now argue that $\langle E + 1 \rangle_n$ remains finite when $n \rightarrow \infty$. Indeed, starting from a meander with $2n$ bridges, we may construct one new meander with $2n + 2$ bridges for each upper and lower exterior arch. As shown in Fig. 11, we simply cut the arch and close it on the other half, thus creating two new bridges and keeping a single connected road. Such

meanders have $2n + 2$ bridges and one single exterior arch on the side where we have closed the arch, and are all distinct. Hence we may write that their number is bounded by M_{n+1} , namely

$$2 \sum_{\substack{\text{meanders } M \\ \text{with } 2n \text{ bridges}}} E(M) \leq M_{n+1} \quad \Rightarrow \quad \langle E \rangle_n \leq \frac{1}{2} \frac{M_{n+1}}{M_n} \rightarrow \frac{R}{2}. \quad (2.30)$$

We therefore have the asymptotic bounds $1 \leq \langle E + 1 \rangle_n \leq 1 + R/2$, which implies that $M_n^{2\text{-riv.}} \propto R^{2n}/n^\alpha$ like ordinary meanders, hence $\alpha_{2\text{-riv.}} = \alpha$. We also deduce that

$$\langle (2p_1 + 1)(2p_2 + 1) \rangle_n \equiv \frac{\sum_{p_1+p_2=n} (2p_1 + 1)(2p_2 + 1) M_{p_1, p_2}}{\sum_{p_1+p_2=n} M_{p_1, p_2}} \sim n^\beta, \quad (2.31)$$

$$\beta = \alpha - \alpha_{2\text{-mark}} = 2 - \Delta_4 = 2 - \frac{1}{24}(\sqrt{14} - \sqrt{5})(\sqrt{5} + \sqrt{29}) = 1.521898 \dots$$

This shows the rather unexpected result that the two-river meanders tend to be very asymmetric, with a number of bridges of the order n on one river (since $p_1 + p_2 = n$) and of the order $n^{\beta-1}$ on the other, with $\beta - 1 = 0.521898 \dots$. The above arguments can be generalized to the case of multi-component meanders and give rise to similar predictions.

In [17], a number of other results have been presented, all corresponding to more sophisticated river geometries, and making use of the magnetic defect operators $\tilde{\psi}_k^{(i)}$. It would also be possible in principle to use mixed operators to generate diagrams with both road and river geometries fixed. Another direction consists in going away from the point $n_1 = n_2 = 0$, for instance by considering the GFPL²($n_1 = 0, n_2 = q$) model in which meanders with arbitrary numbers of roads are considered, with a weight q per road. In that case, the corresponding conformal theory with central charge (2.4)

$$c = -1 - 6 \frac{e^2}{1 - e} \quad e = \frac{1}{\pi} \text{Arccos}\left(\frac{q}{2}\right) \quad (2.32)$$

may be viewed as two decoupled bosonic field theories: a $c = -2$ theory (that of river loops, at $n_1 = 0$) and one with $c = c(q) = 1 - 6e^2/(1 - e)$, where $q = 2 \cos \pi e$ (that of road loops). The generating function $Z_{\text{GFPL}}(q; x, y = 0)$ (2.8) for meander polynomials reads

$$Z_{\text{GFPL}}(q; x, y = 0) = \sum_{n \geq 1} \frac{x^{2n}}{4n} m_n(q) \sim (x_c - x)^{2-\gamma(c)} \quad (2.33)$$

with $\gamma(c)$ as in (2.17), and c as in (2.32). This turns into the asymptotics

$$m_n(q) \sim C(q) \frac{R(q)^{2n}}{n^{\alpha(q)}}, \quad \alpha(q) = 2 - \gamma(c), \quad (2.34)$$

namely [17]

$$\alpha(q) = 2 + \frac{1 - e + 3e^2 + \sqrt{(1 - e + 3e^2)(13 - 13e + 3e^2)}}{6(1 - e)} \quad (2.35)$$

with e as in (2.32). An analogous formula holds for the (multi-component) semi-meander polynomials, namely

$$\bar{m}_n(q) \sim \bar{C}(q) \frac{\bar{R}(q)^n}{n^{\bar{\alpha}(q)}}, \quad \bar{\alpha}(q) = 1 + 2\Delta_1(c) - \gamma(c) \quad (2.36)$$

with $\Delta_1(c)$ as in (2.22), c as in (2.32), and $h_1 = -3/32$ as in (2.23). This yields [17]

$$\bar{\alpha}(q) = 1 + \frac{\sqrt{2(24e^2 + e - 1)}(\sqrt{1 - e + 3e^2} + \sqrt{13 - 13e + 3e^2})}{24(1 - e)} \quad (2.37)$$

with e as in (2.32).

An important remark is in order concerning the range of validity of (2.35) and (2.37). First, the $\text{DPL}^2(0, q)$ model is critical only for $q \leq 2$, i.e. $e \geq 0$. We expect therefore a very different scaling behavior for the meandric numbers when $q > 2$. At large q , it was shown in Ref. [8] that

$$\alpha(q) = \frac{3}{2} \quad (2.38)$$

independently of q .

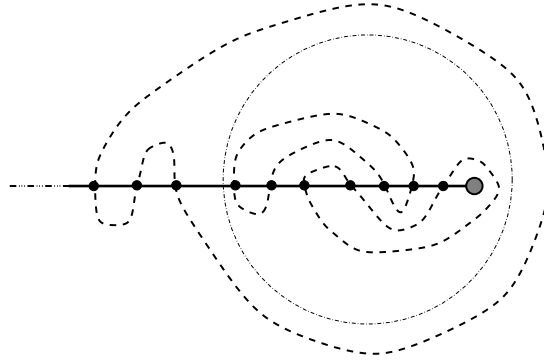


Fig. 12: A typical “branched” semi-meander.

On the other hand, for semi-meanders, this transition at $q = 2$ is never reached. Indeed, another phenomenon appears at a value $q_c < 2$. It corresponds to a proliferation of connected components of road and also of the pieces of road that wind around the source of the river. More precisely, let us compare the two following contributions to the multi-component semi-meander numbers, according to whether:

(i) “branched” semi-meanders dominate: the semi-meander is typically separated into two parts, namely the interior and exterior of a “big circle” as shown in Fig. 12. The contribution of such semi-meanders reads asymptotically

$$\sum_{n_1+n_2=n} \frac{\bar{R}(q)^{n_1}}{n_1^{\bar{\alpha}(q)}} \times \frac{\bar{R}(q)^{n_2}}{n_2^{\bar{\alpha}(q)}} \sim \frac{\bar{R}(q)^n}{n^{2\bar{\alpha}(q)-1}}. \quad (2.39)$$

(ii) “connected” semi-meanders dominate: the semi-meanders cannot be cut as in (i), and typically behave as

$$\frac{\bar{R}(q)^n}{n^{\bar{\alpha}(q)}}. \quad (2.40)$$

The transition between the two regimes (i)-(ii) will take place when $2\bar{\alpha}(q) - 1 = \bar{\alpha}(q)$. We deduce that precisely at the transition, we must have $\bar{\alpha} = 1$, which according to (2.37) takes place when $24e^2 + e - 1 = 0$, namely at the critical value $e = e_c$, $q = q_c$ given by

$$e_c = \frac{\sqrt{97} - 1}{48}, \quad q_c = 2 \cos \pi \frac{\sqrt{97} - 1}{48}, \quad (2.41)$$

also corresponding to $c = 3/4$. Hence the formula (2.37) is only valid for $e_c \leq e$, namely $q \leq q_c = 1.673849 \dots < 2$. Beyond $q = q_c$, we expect the average number of connected components of road to be of the order of n , and we have [8]

$$\bar{\alpha}(q) = 0 \quad \text{for } q > q_c. \quad (2.42)$$

It is quite interesting to notice that the transition of semi-meanders is of a different nature than that of meanders. The latter simply encounters the $q = 2$ transition of the $O(q)$ model. The former undergoes a winding transition, in which semi-meanders become very different from meanders. Indeed, as long as the dominant semi-meanders have very little winding around the source of the river, they behave just like meanders (hence $R(q) = \bar{R}(q)$ in the regime $q < q_c$). But when the winding number of the semi-meanders becomes relevant (of the order of n) we expect many more semi-meanders than meanders with the same number of bridges, and $\bar{R}(q) > R(q)$ for $q > q_c$.

3. Meander enumeration algorithms

In this Section, we will describe the algorithms that we used to check numerically our predictions of Sect. 2 for the different configuration exponents. All the results presented below concern the case $n_1 = 0$, i.e. a connected river configuration, and a varying weight

$n_2 = q$ per road, i.e. multi-connected road configurations. We will also consider the several meander geometries discussed in Sect. 2.

All our algorithms are based on transfer matrix techniques. Transfer matrices have proven to be very powerful for studying a wide range of statistical mechanics systems, especially in two dimensions. Originally applied to systems with local interaction, such as the Ising model, the “row to row” transfer matrix describes the transition between two successive rows of spins, say at ‘time’ t and $t + 1$ along the transfer direction. More recently, the transfer matrix technique was also applied to systems with non-local degrees of freedom, but where, in a suitably designed basis, the statistical weights can still be evaluated between neighboring time slices. In this way it became possible to study self-avoiding polygons [27] and walks [28], and the random cluster model [29], to mention but a few important examples.

Finally, transfer matrices can also be applied to random lattice problems, as long as a definite transfer direction can be defined, as for instance in the case of Lorentzian gravity [30]. This is also precisely the case in the meander problem, where we can simply choose to transfer along the river, adding one bridge in each time step. This was first recognized by Jensen in [10] where the method proved to be much better than previous enumeration algorithms, leading in particular to the largest accessible numbers of bridges.

When implemented on a computer, the transfer matrix algorithms will allow to enumerate *exactly* the various meandric objects that we are interested in for a fixed finite number N of bridges up to a certain maximal value of N (typically up to 48 bridges in the results presented below). From these exact finite N values, we can extract estimates for the large N asymptotic behaviors, and in particular for the configuration exponents described in Sect. 2. We can then compare these estimates to the corresponding expected theoretical values.

This section is organized as follows: The case of one infinite river (the original meander problem) is discussed in subsection 3.1, while the other geometries, including the case of two infinite parallel rivers (connected at infinity), with possibly marked points on each of them, and the case of a semi-infinite river (semi-meanders), are discussed in subsection 3.2. In the three cases above, we allow only crossing vertices of type a (cf. Fig. 1). The inclusion of tangency points for the infinite river case (tangent meanders) is discussed in subsection 3.3.

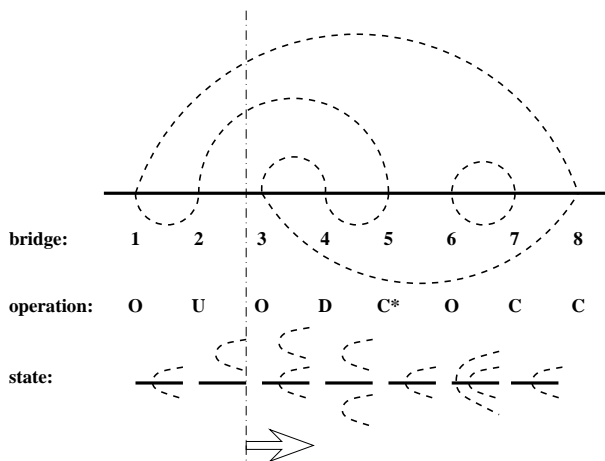


Fig. 13: A multi-road meander with 8 bridges and 2 connected components. Upon addition of a new bridge, four different operations (O, C, U and D) are allowed, as discussed in the text. We also show the state of that part of the meander that is to the left of a given vertical line perpendicular to the river (here in position after $t = 2$ steps). The transfer matrix acts by transferring this line from the left to the right.

3.1. One infinite river (meanders)

Figure 13 shows a typical meander system with one infinite river and $N = 8$ bridges. The partition function is defined by giving a weight $n_2 = q$ to each road. The transfer matrix acts by transferring from the left to the right a vertical line intersecting the river between two consecutive bridges. A *state* characterizes that part of the system that is to the left of the vertical line by listing the pairwise connectivities amongst the road segments as well as the position of the river.

Whenever the vertical line is transferred one step to the right, a new bridge is added and one out of four possible *operations* (O, C, U and D) can take place, as indicated on the figure. Each of these operations connects two consecutive states of the system, before and after the addition of the bridge. The operation O *opens* a new road segment on top of the river, thus connecting the two sides of the river. Similarly the operation C *closes* a road on top of the river. This operation comes in two variants, depending on whether the closed segment was already connected before the addition of the bridge (C) or not (C*). In the former case, the road segment is erased and a non-trivial Boltzmann factor of q must be accounted for. In the latter case, the connectivity is transformed so as to connect the left-over partners of the two road segments that were eliminated. Finally, a road segment immediately below the river can move *up* (operation U), and a segment just above the river can move *down* (operation D).

In order to fully specify the transfer matrix of this problem we need to enumerate the possible connectivity states at a given time. The number of such states determines the size of the memory needed to store information at time $t = n$. We will therefore compute the number $F(n, N)$ of connectivity states after addition of the n -th bridge for any $n = 1, 2, \dots, 2N$ for the case of $2N$ bridges. Also, to implement the calculation of the meander partition function on a computer, one needs to *order* these states so that the entries of the transfer matrix can be accessed by means of a one-to-one mapping between the states and the set of integers $1, 2, \dots, N_{\text{states}}$. Here N_{states} stands for the total number of states encountered in the whole transfer process from the left of the first bridge to the right of the last one. It is also the dimension of the explored state space and depends explicitly on the number $2N$ of bridges added in the whole process. This number will be estimated below while the explicit ordering procedure will be presented at the end of this subsection.

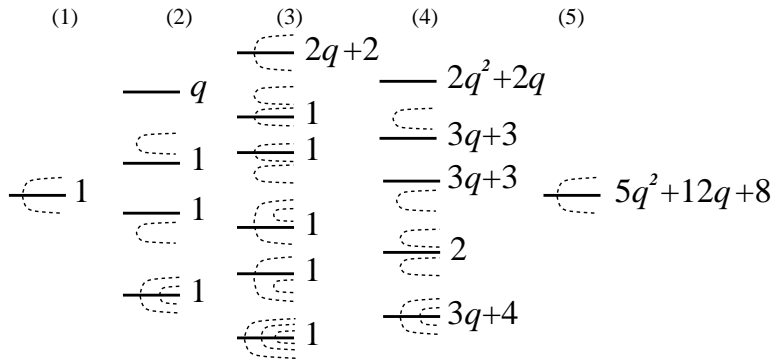


Fig. 14: Transfer matrix enumeration of all multi-road meanders with 6 bridges. The figure lists the complete set of intermediary states after the n -th bridge ($n = 1, 2, \dots, 5$) along with their respective weight.

Before we turn to the general case, let us illustrate the state counting for one infinite river with $2N = 6$ bridges. In Fig. 14, we detail the intermediate steps in the calculation of the corresponding meander polynomial $m_3(q)$. The figure depicts the complete set of states generated by the transfer process, when connecting the “empty” states (vacua) before bridge 1 and after bridge 6, along with their respective weights. Apart from the “empty” states $F(0, 6) = F(6, 6) = 1$, we read $F(1, 3) = 1$, $F(2, 3) = 4$, $F(3, 3) = 6$, $F(4, 3) = 5$, $F(5, 3) = 1$ and $N_{\text{states}} = 11$. The result of the calculation is the meander polynomial $m_3(q) = 5q^3 + 12q^2 + 8q$, indicating that with 6 bridges there are respectively 8, 12 and 5 meanders with 1, 2 and 3 connected components.

Dimension of the state space:

Let us now turn to the computation of the numbers $F(n, N)$. To this end we begin by relating these numbers to properties of a certain class of restricted Brownian walks. Consider a situation where there are p_1 (resp. p_2) road segments above (resp. below) the river, and where these segments are pairwise connected in such a way that exactly h arches cross the river. It is easy to check that the four operations O, C, D and U described above always shift p_1 , p_2 and h by one unit, either $+1$ or -1 , so that, by induction, n , p_1 , p_2 and h have the same parity. Clearly, we also have $h \leq p_1$ and $h \leq p_2$ as an arch crossing the river connects a point above it to a point below it. There are then $(p_1 - h)/2$ (resp. $(p_2 - h)/2$) non-crossing arches that stay above (resp. below) the river. Now, while a crossing arch can be generated by means of a *single* bridge, by using the move O, the generation of a non-crossing arch necessitates at least *two* moves (O followed by either U or D). Therefore, twice the number of non-crossing arches plus the number of crossing arches cannot supersede the number of bridges added, i.e. $p_1 + p_2 - h \leq n$. In terms of h , the arch “height” above the river, this leads to the constraint:

$$\max(0, p_1 + p_2 - n) \leq h \leq \min(p_1, p_2). \quad (3.1)$$

Note that the above condition automatically implies that $p_i \leq n$, $i = 1, 2$.

The above constraint turns out to be the only one as long as $n \leq N$. For $n > N$ there are additional constraints, since we must always be able to annihilate any given state at level n in at most $2N - n$ moves so as to end up with the “empty” state at the right of the $2N$ -th bridge. Since p_1 and p_2 can decrease by at most one at each step, we thus have to impose for $n > N$ the two extra conditions:

$$p_1 \leq 2N - n, \quad p_2 \leq 2N - n. \quad (3.2)$$

It is easy to estimate the number N_{states} of accessible states, i.e. those which satisfy the above constraints (3.1) and (3.2) for all $n = 1, \dots, 2N$. An arch configuration, read from the bottom and upwards, can be mapped onto a $(p_1 + p_2)$ -step Brownian walk, where the position h_i ($i = 0, \dots, p_1 + p_2$) of the walk starts from $h_0 = 0$ and is increased (resp. decreased) by one unit for each opening (resp. closing) of an arch, as illustrated on Figure 15. Evidently these walks are constrained by $h_i \geq 0$ for all i . Decomposing the walk into its left part (describing the arches below the river) and its right part (describing the arches above the river) connected at height h , we are naturally lead to define $f(p, h)$ as

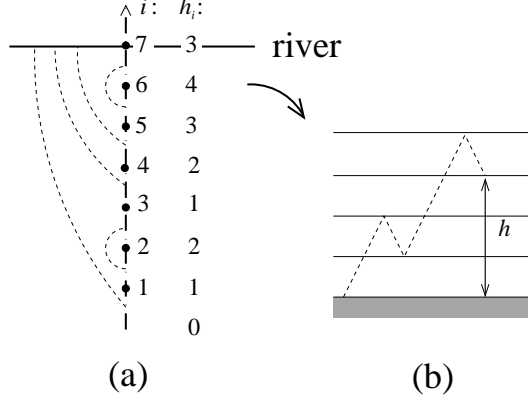


Fig. 15: A typical arch configuration (a) below the river and the corresponding walk (b). The walk has $p = 7$ steps and final height $h = 3$. At each step the height coordinate h_i on (b) changes by ± 1 , according to whether an arch is opened or closed in (a).

the number of walks going from height 0 to height h (or equivalently that of walks going from height h to height 0) in p steps.

To evaluate $f(p, h)$ is a standard exercise. First note that without the constraint $h \geq 0$ this would simply read $\binom{p}{(p-h)/2}$ as we must choose the $(p-h)/2$ ascending steps. Each walk violating the constraint at some point hits $h_i = -1$. Let i be the first time this happens, and consider reversing each step from i and onwards. The result is a walk going from 0 to $(-1) - (h+1)$, or equivalently from 0 to $h+2$. Therefore:

$$f(p, h) = \binom{p}{(p-h)/2} - \binom{p}{(p-h)/2 - 1}. \quad (3.3)$$

In terms of $f(p, h)$, the number $F(n, N)$ of states accessible at level n can then be written as

$$\begin{aligned} F(n, N) &= \sum_{p_1=0}^{\min(n, N-n)} \sum_{p_2=0}^{\min(n, N-n)} \sum_{h=\max(0, p_1+p_2-n)}^{\min(p_1, p_2)} f(p_1, h) f(p_2, h) \\ &= \sum_{h=0}^n \sum_{p_1=h}^{\min(n, 2N-n)} \sum_{p_2=h}^{\min(n+h-p_1, 2N-n)} f(p_1, h) f(p_2, h), \end{aligned} \quad (3.4)$$

where it is implicitly understood that h , p_1 and p_2 in the sums above all have the parity of n .

When $N \geq n$ it is possible to rewrite Eq. (3.4) in a simpler form, since the second constraint in the upper limit of the summations over p_1 and p_2 (namely $p_i \leq N - n$) does

not come into play. Setting $p_1 + p_2 = 2p$, we simply have to enumerate all the set of p arches, cut by the river at a height h that has the same parity as n and satisfies the constraint $h \geq 2p - n$. Let us define

$$h_{\min}(n, p) \equiv \begin{cases} \max(0, 2p - n) & \text{for } n \text{ even} \\ \max(1, 2p - n) & \text{for } n \text{ odd.} \end{cases} \quad (3.5)$$

In the walk language, we have to count all the walks of length $2p$ that stay non-negative with a *marking* at a point of height $h \geq h_{\min}$ and with a well defined parity, that of n . The total number of non-negative walks of length $2p$ going from 0 to 0 and with a marked point at position h can be easily calculated to be:

$$g(p, h) = f(2p, 2h) + f(2p, 2h + 2) = \binom{2p}{p-h} - \binom{2p}{p-h-2}. \quad (3.6)$$

Summing over the heights $h \geq h_{\min}(n, p)$ having the parity of n (which is also that of $h_{\min}(n, p)$) we have

$$\sum_{\substack{h=h_{\min}(n,p) \\ h=h_{\min}(n,p) \bmod 2}}^n g(p, h) = \binom{2p}{p-h_{\min}(n,p)}. \quad (3.7)$$

The complete number of states used in the transfer matrix is now simply obtained by summing over the number of arches. Depending on the parity of n , we get:

$$F(n, N \geq n) = \sum_{p=0}^n \binom{2p}{\min(p, n-p)} \quad \text{for } n \text{ even,} \quad (3.8)$$

and similarly:

$$F(n, N \geq n) = \sum_{p=1}^n \binom{2p}{\min(p-1, n-p)} \quad \text{for } n \text{ odd.} \quad (3.9)$$

Note that the above expressions *do not depend* on N . This is because we assumed that $n \leq N$, in which case the second constraint (3.2) is ineffective. For large n , the above expressions for $F(n, N \geq n)$ can be evaluated by a simple saddle point approximation. Setting $p = yn$, we get a saddle point at a value y^* solution of

$$(3y^* - 1)^3 = (1 - y^*)(2y^*)^2, \quad (3.10)$$

namely with the numerical value $y^* = 0.611491992 \dots$. This value indicates that the state statistics is indeed governed by arch systems with a number $p = p_1 = p_2 = p^* \equiv y^*n$ of arches. The quantity $F(n, N \geq n)$ is then found to grow asymptotically as a^n , where

$$a = \frac{(2y^*)^{2y^*}}{(1 - y^*)^{1-y^*} (3y^* - 1)^{3y^*-1}} , \quad (3.11)$$

which, using (3.10), is also the solution of

$$a^3 = (1 + a)^2 . \quad (3.12)$$

This yields the numerical value $a = 2.147899036 \dots$.

N	$F(N, N)$	$F(n_{\max}, N)$	n_{\max}	N	$F(N, N)$	$F(n_{\max}, N)$	n_{\max}
1	1	1	1	13	12905	26770	15
2	4	4	2	14	27971	62959	16
3	6	6	3	15	59282	155153	18
4	16	16	4	16	128130	388695	19
5	29	29	5/6	17	272610	950128	20
6	68	68	6	18	588153	2279273	21
7	134	161	8	19	1254586	5733997	23
8	300	363	9	20	2703503	14523043	24
9	614	846	10	21	5777115	35946838	25
10	1349	1890	11	22	12438708	87192966	26
11	2813	4579	13	23	26613942	223196395	28
12	6126	11216	14	24	57268474	568622062	29

Table 1: Number of intermediate states employed by the transfer matrix algorithm for multi-road meanders with $2N$ bridges. The number of states $F(N, N)$ after addition of the N -th bridge is less than the maximal number of states $F(n_{\max}, N)$, which occurs at a value n_{\max} slightly above N .

In Table 1, we give some explicit values of the number of states needed when enumerating meanders with $2N$ bridges. It is seen that the maximum number of states occurs slightly after the addition of the middle bridge, $n = N$. For large N , one can easily estimate the value n_{\max} of n where this maximum occurs. Indeed, for $n > N$, the second condition (3.2) starts to play a role. As we have seen, for large n , the state statistics without the second constraint is dominated by arch configurations with $p_1 = p_2 = p^* = y^*n$. Therefore,

we expect this second constraint (3.2) to effectively affect the asymptotic behavior and start reducing the number of states whenever $p^* = 2N - n$, i.e. for $n = 2N/(1 + y^*)$. Assuming that this precisely corresponds to the step having the maximum number of states, we have

$$n_{\max} = 2N/(1 + y^*) = 1.241085907 \cdots N . \quad (3.13)$$

We can then estimate the asymptotic number of encountered states in the whole process to grow like:

$$N_{\text{states}} \sim F(n_{\max}, N) \sim a^{n_{\max}} = (2.582603447 \cdots)^N . \quad (3.14)$$

The estimates (3.13) and (3.14) agree with the values observed in Table 1.

Ordering the states:

According to Eq. (3.4), the full set of $F(n, N)$ states can be ordered if we know how to order the $f(p, h)$ restricted Brownian walks defined above. Namely, in that case one can order the complete set of states lexicographically after h , p_1 , p_2 , the value of the first Brownian walk $[1, 2, \dots, f(p_1, h)]$, and finally the value of the second Brownian walk $[1, 2, \dots, f(p_2, h)]$. By this we mean simply that state A precedes state B if $h_A < h_B$. If $h_A = h_B$ this criterion is inconclusive, and one compares the values of p_1 , so that A precedes B if $p_{1,A} < p_{1,B}$. In case of further equality one proceeds to compare p_2 , and so on.

To order the Brownian walks, consider first the example contributing to $f(7, 3)$ shown in Fig. 15. The idea is to obtain another formula for $f(p, h)$ which will in turn allow us to define a recursive ordering of the walks. We start by focusing on the first (lowermost) arch. Either this arch is open (as is the case on the figure), or it closes at some other point before p . In the first case the remaining arch configuration is a contribution to $f(p - 1, h - 1)$, and in the second the arches inside the first arch are independent of the arches above its termination point. We therefore have

$$f(p, h) = f(p - 1, h - 1) + \sum_{k=1,3,5,\dots} f(k - 1, 0) f(p - k - 1, h) , \quad (3.15)$$

with $f(0, h) = \delta_{0,h}$, and $f(p, h) = 0$ for $p < 0$. This is the required formula.

A walk contributing to $f(p, h)$ can now be recursively ordered, first by considering the termination point of the lowermost arch (which by definition is infinity if that arch is open), then by (recursively) considering the ordering of the smaller arch system inside the first arch, and finally by (recursively) considering the ordering of the arch system above the first arch (which only exists if that arch is closed). The procedure just described generalizes the ordering of the Catalan connectivities $c_{p/2} = f(p, 0)$ given in Ref. [29].

3.2. Other geometries

We now come to the case of the more involved meandric geometries encountered in Sect. 2.

Two infinite rivers:

It is possible to generalize the multi-road one-river transfer matrix to the case of several rivers, provided that the latter can be deformed into a system of parallel lines that are only connected among themselves at infinity. For simplicity we consider in the following the case of two such infinite rivers. As we have seen, this situation also corresponds to the deformation of the figure-eight configuration shown in Fig. 9, provided that a marked point is added on each river.

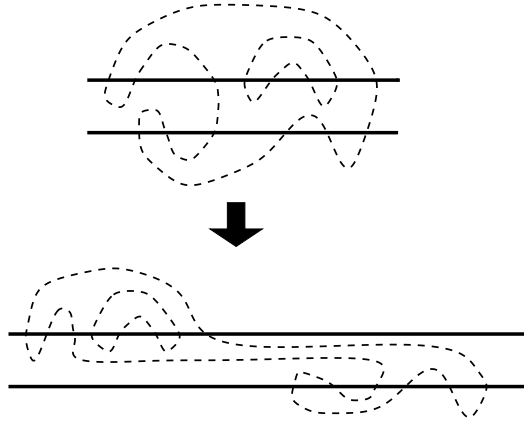


Fig. 16: The deformation of a two-river configuration by sending all the bridges crossing the upper river to the left and all the bridges crossing the lower river to the right. The transfer matrix acts by first adding the left bridges, then the right ones.

As before, the crucial point is to have a well-defined transfer direction, which we simply take to be parallel to both rivers. For any given configuration with $2N$ bridges we write $N = N_1 + N_2$, where $2N_1$ (resp. $2N_2$) is the number of times the roads cross the first (resp. the second) river. Note that contrary to the bridges on the same river which are naturally ordered, bridges on the first and on the second river are not naturally ordered with respect to one another. To avoid double counting in the transfer matrix approach, we can simply deform the roads as in Fig. 16 so as to send all the bridges of river 1 to the left and all those of river 2 to the right. In the transfer process, we thus add first the $2N_1$ bridges crossing the first river and then the $2N_2$ bridges crossing the second river.

Given a decomposition $N = N_1 + N_2$, the calculations therefore proceed exactly as in the one-river case, except that when both $N_1 > 0$ and $N_2 > 0$ not *all* of the connectivity states described in Sect. 3.1 come into use. Denoting by p_1 the number of road segments above the first river, by p_2 the road segments in between rivers, and by p_3 the segments below the second river, we now have the following constraints after the addition of the n -th bridge:

$$\begin{aligned} p_1 &\leq \max(\min(n, 2N_1 - n), 0), \\ p_2 &\leq \min(n, 2N - n), \\ p_3 &\leq \max(\min(n - 2N_1, 2N - n), 0). \end{aligned} \tag{3.16}$$

The total two-river meander polynomial is obtained by summing over the possible decompositions. We can furthermore simply address the situation with a marked point on either river by weighing each term in the decomposition by a factor of $(2N_1 + 1)(2N_2 + 1)$.

One semi-infinite river (semi-meanders):

Finally, we have examined systems of semi-meanders, where the roads are allowed to wind around the source of a semi-infinite river. Each winding number w can be examined separately, by choosing an initial state of w arches nested inside one another, and simply applying the four operations discussed in Sect. 3.1. Unfortunately in this situation we have not found a simple and full description of the generated states (apart from $w = 0$ and $w = 1$). It is however still possible to carry out the transfer matrix calculations, by simply inserting the generated states in an unordered list. The price to be paid is that to find a given state one will have to sequentially search through the entire list, leading to a pitiful waste of computation time. This is nevertheless what we have done, and consequentially we have had to content ourselves with smaller system sizes.

3.3. Tangency points

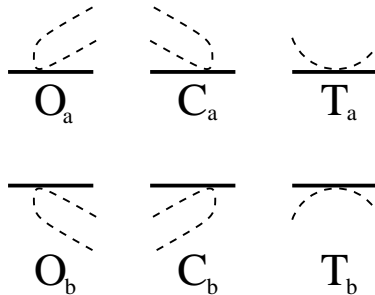


Fig. 17: The six new operations allowed for tangent meanders.

We have also enumerated systems of *tangent* meanders, where apart from the four types of moves at each bridge described in subsection 3.1, we allow for the six additional operations depicted in Figure 17. These moves allow to *open* a road whilst staying *above* or *below* the river (O_a and O_b), to similarly *close* a road without crossing the river (C_a and C_b), and finally to *touch* the river whilst staying *above* it or *below* it (T_a and T_b). The meander polynomial is now defined by assigning a weight x to each of the crossing bridges and a weight y to each of the tangent vertices.

Here again, we have not been able to find an explicit way of enumerating and ordering the states obtained by applying this set of ten operations to the vacuum.

4. Numerical results

Let us now present our numerical results obtained by use of the algorithms presented in Sect. 3, together with an appropriate extrapolation procedure. Subsection 4.1 discusses multi-component meanders and introduces the extrapolation method. Subsection 4.2 is devoted to the case of two parallel rivers, while subsection 4.3 addresses semi-meanders. Finally, we study tangent meanders in subsection 4.4.

4.1. One infinite river (meanders)

We have enumerated multi-connected meanders with one infinite river and a *fixed fugacity* q up to $N = 24$, i.e. $2N = 48$ bridges for $q = 0, \sqrt{2}, \sqrt{3}$ and 2. In other words, we evaluated the quantities $M_N = \lim_{q \rightarrow 0} (m_N(q)/q)$, $m_N(\sqrt{2})$, $m_N(\sqrt{3})$ and $m_N(2)$ for $N = 1, \dots, 24$. From these numbers, we can extract estimates for the large N “activity” per bridge $R(q)$ and configuration exponent $\alpha(q)$ defined as in Eq. (2.11) by :

$$m_N(q) \sim C(q) \frac{R(q)^{2N}}{N^{\alpha(q)}} . \quad (4.1)$$

The estimates for $\alpha(q)$ can be transformed into estimates for the central charge $c(q)$ through the following relation, inverting (2.17) for $\gamma = 2 - \alpha(q)$:

$$c(q) = 1 - 6 \frac{(2 - \alpha(q))^2}{(\alpha(q) - 1)} . \quad (4.2)$$

Starting from the zero-th order values:

$$\begin{aligned} R_N^{(0)}(q) &\equiv \sqrt{\frac{m_{N+1}(q)}{m_N(q)}} \\ \alpha_N^{(0)}(q) &\equiv (N + 1)^2 \left(\frac{m_{N+2}(q)m_N(q)}{(m_{N+1}(q))^2} - 1 \right) , \end{aligned} \quad (4.3)$$

we can build better estimates $R_N^{(p)}$ and $\alpha_N^{(p)}$ by a recursive use of a standard convergence acceleration procedure:

$$R_N^{(p)} = R_N^{(p-1)} - \frac{p+1}{p} \frac{(R_{N+1}^{(p-1)} - R_N^{(p-1)})(R_N^{(p-1)} - R_{N-1}^{(p-1)})}{R_{N+1}^{(p-1)} + R_{N-1}^{(p-1)} - 2R_N^{(p-1)}} \quad (4.4)$$

and similarly for $\alpha_N^{(p)}$. The procedure implicitly assumes that the corrections to the asymptotic scaling (4.1) are regular, i.e. integer powers of $1/N$, in which case it guarantees that $R_N^{(p)}(q) = R(q) + \mathcal{O}(1/N^{p+1})$.

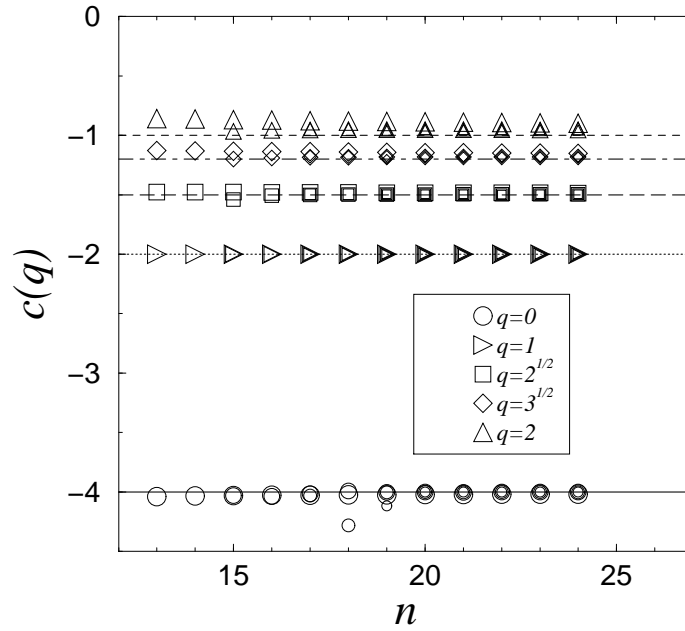


Fig. 18: The estimated central charge obtained from the values $\alpha_N^{(p)}(q)$ with $p = 1, 2, 3$ and 4 iterations. The size of the symbols decreases with the number of iterations. Each value is represented at an abscissa n corresponding to the largest index $N = n$ of $m_N(q)$ used in the estimate. We also draw horizontal lines at the predicted values of $c(q)$.

Fig. 18 shows the estimated central charge obtained through (4.2) using $\alpha_N^{(p)}(q)$ for $p = 1, 2, 3, 4$, together with the expected central charge according to (2.4) with $n_1 = 0$ and $n_2 = q$. For completeness, we also show the corresponding estimates obtained for $q = 1$ with $m_N(1) = (c_N)^2$ in terms of the Catalan numbers c_N . The corresponding quantitative values are displayed in Table 2 below.

q	$\alpha_{\text{theor.}}(q)$	$\alpha_{\text{num.}}(q)$	$R_{\text{num.}}^2(q)$	$c_{\text{theor.}}(q)$	$c_{\text{num.}}(q)$
0	$\frac{29+\sqrt{145}}{12} = 3.4201328\dots$	3.4207	12.26286	-4	-4.003
1	3	3.00000	16.000000	-2	-2.0000
$\sqrt{2}$	$\frac{53+\sqrt{265}}{24} = 2.8866175\dots$	2.885	17.52468	-3/2	-1.496
$\sqrt{3}$	$\frac{131+\sqrt{1441}}{60} = 2.8160084\dots$	2.812	18.68970	-6/5	-1.18
2	$\frac{13+\sqrt{13}}{6} = 2.7675918\dots$	2.75	19.669	-1	-0.95

Table 2: Numerical estimates for the meander configuration exponent $\alpha(q)$, the activity $R^2(q)$ per pair of bridges, and the central charge $c(q)$. The error is implicitly on the last digit. The corresponding theoretical values are also listed.

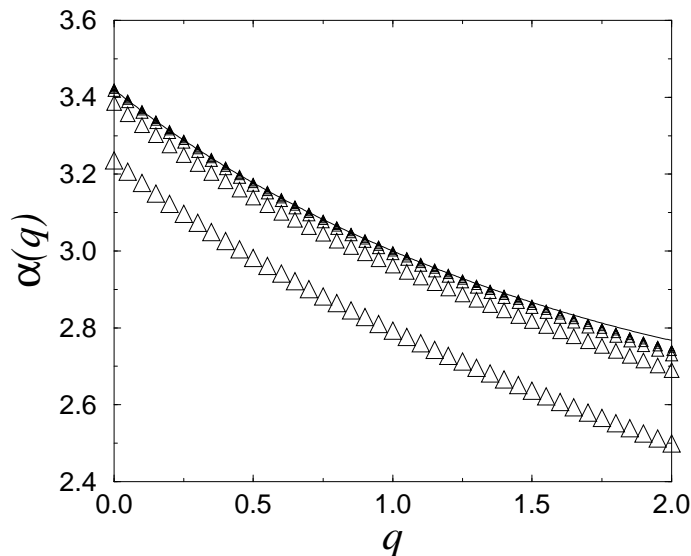


Fig. 19: Numerical estimates (triangles) for the meander configuration exponent $\alpha(q)$ for $0 \leq q \leq 2$, together with the predicted value (2.35)-(2.32) (solid line). We display the result of several iterations of our convergence acceleration procedure. The size of the symbols decreases with the number of iterations.

We have also computed the numbers $M_N^{(k)} = \mu_{2N,0}^{(k)}$ of meanders with one infinite river, $2N$ bridges and a fixed number k of connected components ($k = 1, \dots, N$) for $N = 1, \dots, 20$ (40 bridges). As an illustration we display the results for $N = 20$ in Table 3 below.

k	$M_{20}^{(k)}$	k	$M_{20}^{(k)}$
1	64477712119584604	11	706958959835806990
2	511563350415103008	12	235265604762448572
3	1901345329566422790	13	64713641205591820
4	4405839231880790648	14	14658557362753320
5	7145814923879522986	15	2709804590263296
6	8632733743310196256	16	402058856155712
7	8070705247685170684	17	46500885666900
8	5988061883039308848	18	3978168316200
9	3587066097601934530	19	226760523600
10	1755310029771295216	20	6564120420

Table 3: Multi-component meander numbers $M_N^{(k)}$ with $2N = 40$ bridges and k connected components of road, $k = 1, 2, \dots, 20$.

From these values, we can extract the polynomials $m_N(q) = \sum_{k=1}^N M_N^{(k)} q^k$, hence the values $R(q)$ and $\alpha(q)$ for a *varying fugacity* q . These values are displayed in Fig. 19 together with the prediction (2.35)-(2.32).

All our estimates clearly validate the theoretical predictions with a very good accuracy. We note a small discrepancy for values of q close to $q = 2$. This corresponds to the regime which has the worst convergence of our acceleration procedure. This poor convergence might be due to either corrections which are not regular, as implicitly assumed, or to the vicinity of a transition at $q = 2$ where the DPL² model stops being critical. We anyway impute this small discrepancy to our estimation procedure.

4.2. Two infinite rivers

Beyond the central charge, we can also test the operator content of the theory. A first check concerns the dimension Δ_4 of the operator creating a vertex with four outgoing river segments, which, as we already explained, can be measured through the configuration exponent $\alpha_{2\text{-mark}}$ for two parallel infinite rivers with a marked point on each river. As we mentioned before, in the absence of marking, we expect the two-river configuration exponent $\alpha_{2\text{-riv.}}(q)$ to be simply the same as that of meanders with a single infinite river.

Fig. 20 and 21 show our results based on enumerations with up to $2N = 42$ bridges for fixed $q = 0, \sqrt{2}, \sqrt{3}$ and 2. For completeness, we also added estimates for $q = 1$, as

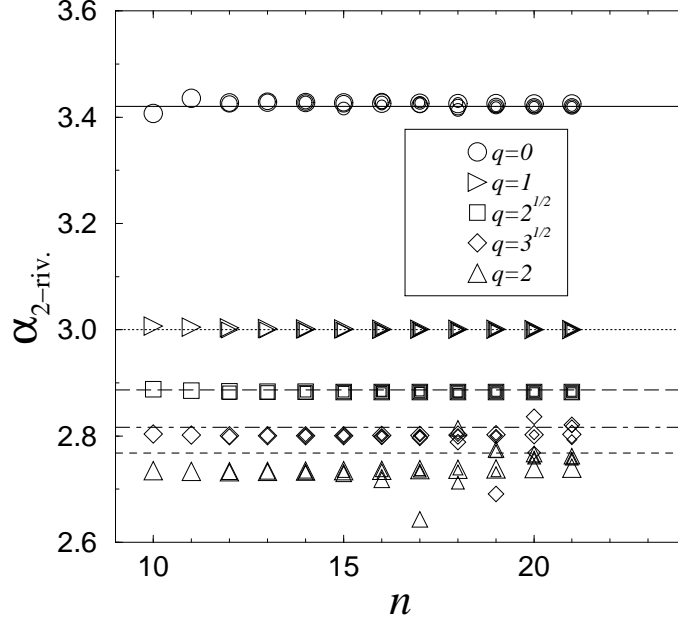


Fig. 20: The estimated configuration exponent for two *un-marked* rivers, obtained with $p = 1, 2, 3$ and 4 iterations of the acceleration procedure (4.4). The size of the symbols decreases with the number of iterations. Each value is represented at an abscissa n corresponding to the largest index $N = n$ of $m_N^{2-\text{riv.}}(q)$ used in the estimate. We also draw horizontal lines at the predicted values of $\alpha_{2-\text{riv.}}(q)$.

extracted from the exact expressions:

$$m_N^{2-\text{riv.}}(q = 1) = \sum_{p=0}^N c_p c_{N-p} c_N = c_N c_{N+1} \quad (4.5)$$

for two un-marked rivers, and

$$m_N^{2-\text{mark}}(q = 1) = \sum_{p=0}^N (2p + 1)(2(N - p) + 1) c_p c_{N-p} c_N = c_N \left(4^{N+1} - \binom{2n+3}{n+1} \right) \quad (4.6)$$

for two marked rivers. Note that in this latter case of two marked rivers, the leading contribution $m_N^{2-\text{mark}}(1) \sim (16)^N / N^{3/2}$ is corrected by a sub-leading contribution $\sim (16)^N / N^2$, with an exponent displaced by a half-integer. In this case, the corrections to the leading term thus involve generically half-integers instead of integers. We expect this phenomenon to be generic for all values of q with a double expansion involving both the exponent $\alpha_{2-\text{mark}}(q)$ and its “descendants” shifted by integers, and a sub-leading correction with the exponent $\alpha_{2-\text{riv.}}(q) - 1$ and its descendants. Since $\alpha_{2-\text{riv.}} - 1 - \alpha_{2-\text{mark}}$ is always close

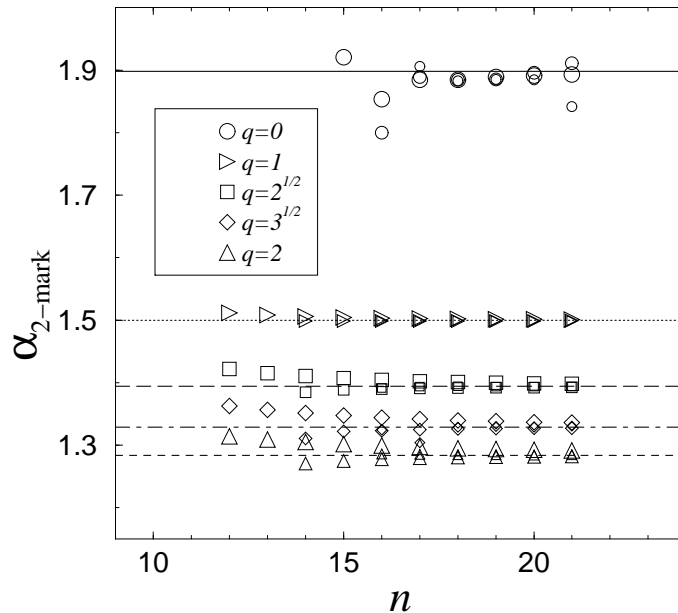


Fig. 21: The estimated configuration exponent for two *marked* rivers, obtained with $p = 2, 3$ and 4 iterations of the (modified, as explained in the text) acceleration procedure. The size of the symbols decreases with the number of iterations. Each value is represented at an abscissa n corresponding to the largest index $N = n$ of $m_N^{2-\text{mark}}(q)$ used in the estimate. We also draw horizontal lines at the predicted values of $\alpha_{2-\text{mark}}(q)$.

to $1/2$ for the values of q of interest, we decided to use a modified acceleration procedure

assuming half-integer corrections to scaling (the index p in (4.4) now takes half-integer

values). The estimates of Table 4 and Fig. 21 have been obtained with this modified

procedure.

q	$\alpha_{2\text{-riv.}}(q)$	$\alpha_{\text{num.}}(q)$	$R_{\text{num.}}^2(q)$
0	$\frac{29+\sqrt{145}}{12} = 3.4201328\dots$	3.4205	12.2627
1	3	3.00000	16.000000
$\sqrt{2}$	$\frac{53+\sqrt{265}}{24} = 2.8866175\dots$	2.882	17.5246
$\sqrt{3}$	$\frac{131+\sqrt{1441}}{60} = 2.8160084\dots$	2.80	18.688
2	$\frac{13+\sqrt{13}}{6} = 2.7675918\dots$	2.75	19.663
q	$\alpha_{2\text{-mark}}(q)$	$\alpha_{\text{num.}}(q)$	$R_{\text{num.}}^2(q)$
0	$\frac{\sqrt{5}+\sqrt{14}}{\sqrt{29}-\sqrt{5}} = 1.8982348\dots$	1.89	12.26
1	3/2	1.499	15.9999
$\sqrt{2}$	$\frac{\sqrt{5}+\sqrt{23}}{\sqrt{53}-\sqrt{5}} = 1.3941001\dots$	1.393	17.527
$\sqrt{3}$	$\frac{\sqrt{11}+\sqrt{56}}{\sqrt{131}-\sqrt{11}} = 1.3285858\dots$	1.33	18.69
2	$\frac{\sqrt{11}+\sqrt{2}}{\sqrt{26}-\sqrt{2}} = 1.2838772\dots$	1.28	19.67

Table 4: Numerical estimates for the configuration exponent and the activity $R^2(q)$ per pair of bridges in the case of two un-marked rivers (upper half) and two marked rivers (lower half). The error is implicitly on the last digit. The corresponding theoretical values are also listed.

Here again, the numerical values corroborate our predictions for the various configuration exponents. Note that we find that the activity per bridge is for these two cases the same as for a single infinite river. It should not come as a surprise that the activity $R(q)$ per bridge is independent of the particular meander geometry since it is a bulk quantity insensitive to the choice of boundary conditions (river shapes). It is also interpreted as the inverse of the convergence radius common to all the generating functions of the numbers at hand, also viewed as various correlators within the same theory.

4.3. One semi-infinite river (semi-meanders)

As a second check of the operator dimensions of the theory, we also considered the case of semi-meanders with a single semi-infinite river ($n_1 = 0$) and an arbitrary number k of connected components of road. Our estimates rely on an exact enumeration of the numbers $\bar{M}_N^{(k)}(w)$ of semi-meanders with N bridges, k roads and winding number w for $1 \leq N \leq 33$, $1 \leq k \leq N$, $0 \leq w \leq N$ and $w = N \pmod{2}$. For illustration, we list in Table 5 below respectively the numbers $\bar{M}_{33}^{(k)} = \sum_w \bar{M}_{33}^{(k)}(w)$ of semi-meanders with $N = 33$ bridges and k roads (irrespective of the winding numbers) as well as the numbers $\bar{M}_{33}^{(1)}(w)$ of connected semi-meanders with winding number $w = 1, 3, 5, \dots, 33$.

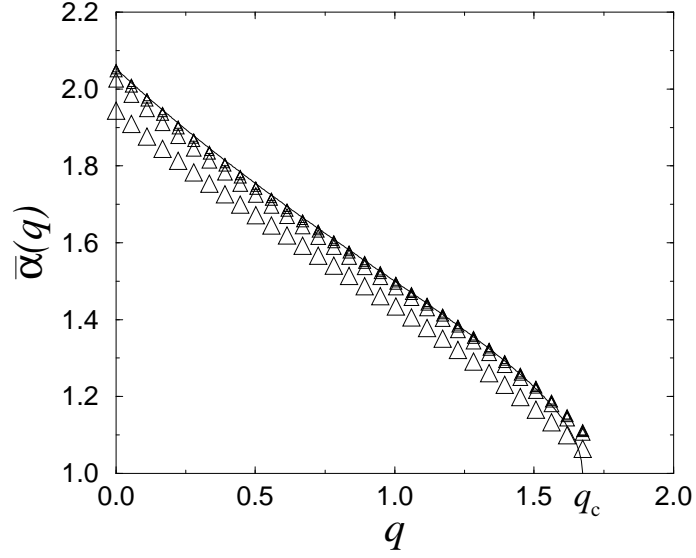


Fig. 22: Numerical estimates for the semi-meander configuration exponent $\bar{\alpha}(q)$ for $0 \leq q \leq q_c$, together with the predicted value (2.37)-(2.32). We display the result of several iterations of the acceleration procedure. The size of the symbols decreases with the number of iterations.

k	$\bar{M}_{33}^{(k)}$	k	$\bar{M}_{33}^{(k)}$
1	455792943581400	18	3659252585228
2	3285874327160852	19	1040041120124
3	11119764476127424	20	279039302088
4	23598381333433844	21	70513532334
5	35436190513634790	22	16729859124
6	40334792072264540	23	3710923316
7	36464182713722576	24	765325248
8	27136413723456560	25	145710912
9	17127401092409102	26	25374900
10	9409371247346540	27	3992846
11	4602479751584184	28	558396
12	2042918178657320	29	67804
13	835326688674886	30	6904
14	318096906554664	31	557
15	113643690324368	32	32
16	38261586556480	33	1
17	12168938393766		
w	$\bar{M}_{33}^{(1)}(w)$	w	$\bar{M}_{33}^{(1)}(w)$
1	59923200729046	19	16277801502
3	121544501379440	21	1326698396
5	125267070807626	23	73827420
7	85716694410306	25	2638462
9	42336073574012	27	55052
11	15599486790514	29	568
13	4337132101822	31	2
15	908960663970	33	0
17	142142103262		

Table 5: Multi-component semi-meander numbers $\bar{M}_N^{(k)}$ with $N = 33$ bridges and k connected components of road, $k = 1, 2, \dots, 33$, and fixed winding connected semi-meander numbers $\bar{M}_N^{(1)}(w)$ with $N = 33$ and $w = 1, 3, 5, \dots, 33$.

For this particular geometry, a clear parity effect occurs and it is thus important to make numerical evaluations from semi-meander numbers with either even or odd N to

avoid large numerical errors. The results presented in Fig. 22 were extracted from even values of N . Table 6 lists quantitative values for the configuration exponent and the activity per pair of bridges. Here again, we note that the activity per bridge is identical to that of the other geometries. As shown in Fig. 22, the configuration exponent is in very good agreement for q less than 1.5. For larger values of q , a small discrepancy appears, again imputable to a poor convergence probably due to the vicinity of a transition point, now at $q = q_c$ where we expect a proliferation of connected components of road for the semi-meander geometry.

q	$\bar{\alpha}_{\text{theor.}}(q)$	$\bar{\alpha}_{\text{even}}(q)$	$\bar{\alpha}_{\text{odd}}(q)$	$\bar{R}_{\text{even}}^2(q)$	$\bar{R}_{\text{odd}}^2(q)$
0	$1 + \frac{\sqrt{11}(\sqrt{29} + \sqrt{5})}{24} = 2.0531987\dots$	2.0532	2.051	12.26287	12.2626
1	3/2	1.500000	1.500000	16.000000	16.000000
$\sqrt{2}$	$1 + \frac{\sqrt{2}}{48}(\sqrt{53} + \sqrt{5}) = 1.2803730\dots$	1.282	1.282	17.5247	17.5247

Table 6: Numerical estimates for the configuration exponent and the activity $R^2(q)$ per pair of bridges in the case of one semi-infinite river (semi-meanders). The error is implicitly on the last digit. The corresponding theoretical values are also listed.

4.4. Tangent meanders

Finally, we also checked our assertion that the “tangency” vertices of type b (see Fig. 1) are irrelevant. We computed the canonical partition function $\mu_N(q; x, y)$ defined in (2.10) for the particular case of tangent meanders with a single connected component of road ($q = 0$), a fixed weight $x = 1$ for “crossing” vertices and with several values of the weight y per “tangency” vertex. We enumerated up to $N = 24$ vertices for $y = 0.5, 1$ and 2 while $y = 0$ simply corresponds to the meander configurations of subsection 4.1 for which we have results up to 48 vertices.

Our results are represented in Fig. 23 and the corresponding quantitative values listed in Table 7 below. We find a clear evidence that the configuration exponent is independent of y , indicating that the universality class of tangent meanders and that of meanders are the same, as predicted in subsection 2.3.

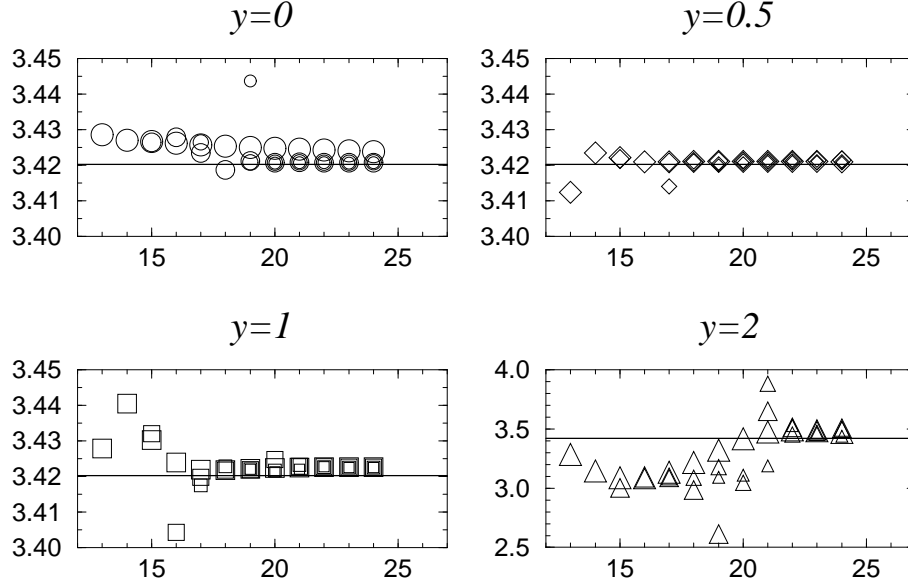


Fig. 23: The estimated configuration exponent α for tangent meanders with a weight $y = 0, 0.5, 1$ and 2 per tangency vertex. The size of the symbols decreases with the number p of iterations (here $p = 1, 2, 3, 4$). Each value is represented at an abscissa n corresponding to the largest index $N = n$ for the number of vertices (resp. the number of bridge pairs in the case $y = 0$) used in the estimate. We also draw horizontal lines at the predicted value.

y	$\alpha_{\text{theor.}}$	$\alpha_{\text{num.}}(y)$	$R_{\text{num.}}(y)$
0	$\frac{29+\sqrt{145}}{12} = 3.4201328\dots$	3.4207	3.50184
1/2	$\frac{29+\sqrt{145}}{12} = 3.4201328\dots$	3.4208	6.188
1	$\frac{29+\sqrt{145}}{12} = 3.4201328\dots$	3.422	8.735
2	$\frac{29+\sqrt{145}}{12} = 3.4201328\dots$	3.4	13.63

Table 7: Numerical estimates for the configuration exponent and the activity $R(q)$ per bridges in the case of tangent meanders with $q = 0$, $x = 1$ and $y = 0, 0.5, 1$ and 2 . The error is implicitly on the last digit. The corresponding theoretical value is also listed.

5. Discussion and conclusion

In this paper, we have presented theoretical and numerical evidence for a number of exact meandric configuration exponents. Although the sequence of physical arguments leading to the exact predictions is by no means a mathematical proof, the numerical evidence is compelling. Let us add a few comments on possible generalizations of our work.

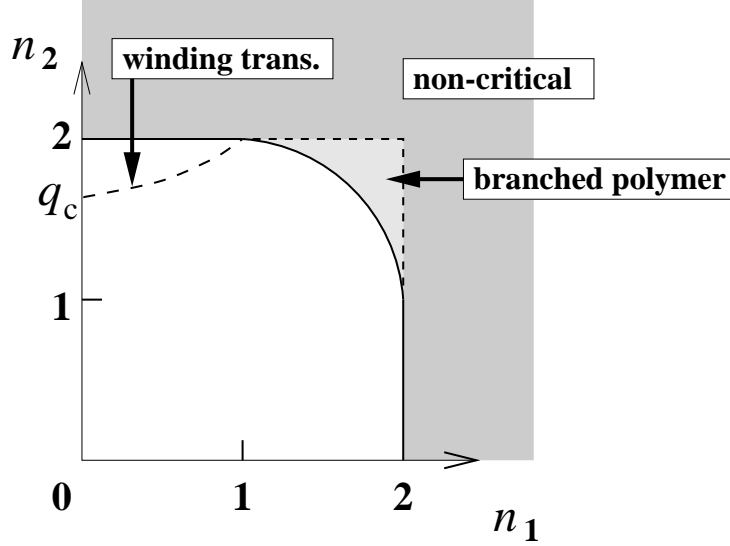


Fig. 24: The range of validity of the exact prediction for the meander configuration exponent in the general case of a weight n_1 per river and n_2 per road. In addition to the criticality constraint that $0 \leq n_i \leq 2$, we have represented the $c(n_1, n_2) = 1$ curve (joining the points $(n_1 = 2, n_2 = 1)$ and $(n_1 = 1, n_2 = 2)$, and passing by $(n_1 = \sqrt{2}, n_2 = \sqrt{2})$), beyond which the meanders are in a branched polymer phase. We have also represented by a dashed line the location of the winding transition joining the point $(0, q_c)$ to the point $(1, 2)$.

5.1. Ranges of validity and transitions

The physical arguments presented above allow to go much farther than just the case of one or two rivers. Indeed, we have seen that meanders are a particular case of the $\text{GFPL}^2(n_1, n_2)$ model at $n_1 = n_2 = 0$ with $y = 0$. Let us define multi-river and multi-road meander polynomials of order n , $m_n(n_1, n_2)$, by the following expansion of the partition function Z_{GFPL} (2.5) for $y = 0$

$$Z_{\text{GFPL}}(n_1, n_2; x) = \sum_{n \geq 1} \frac{x^{2n}}{4n} m_n(n_1, n_2) . \quad (5.1)$$

Then we can as well predict the following large n asymptotic behavior

$$m_n(n_1, n_2) \sim C(n_1, n_2) \frac{R(n_1, n_2)^{2n}}{n^{\alpha(n_1, n_2)}} , \quad \alpha(n_1, n_2) = 2 - \gamma(c(n_1, n_2)) , \quad (5.2)$$

where $c(n_1, n_2)$ is the central charge of the $\text{DPL}^2(n_1, n_2)$ model (2.4), and $\gamma(c)$ is as in (2.17). The general prediction (5.2) was actually proved in the case $n_1 = 1$ and arbitrary $0 \leq n_2 \leq 2$ in [15], by solving a particular matrix model.

Note however that the range of validity of (2.17) imposes that $c(n_1, n_2) \leq 1$. This gives the total range of validity of Fig. 24. Outside of this range, we must consider the two following cases:

- (i) One of the $n_i > 2$: then the DPL² model is no longer critical, and we have no field theoretical prediction as to the value of the configuration exponent. It has been shown however, using matrix model techniques, that in the resembling case of the so-called $O(n)$ model, the critical exponent takes a constant value $\alpha = 3/2$ independently of $n > 2$ [16].
- (ii) Both $n_1, n_2 \leq 2$ but $c(n_1, n_2) > 1$: one encounters the well-known “c=1 barrier” phenomenon in two-dimensional quantum gravity [31]. The corresponding theories are dominated by configurations of surfaces with long fingers (branched polymer phase of quantum gravity). Remarkably, it was shown that $\gamma = 1/2$ throughout this phase, leading also to a constant exponent $\alpha = 3/2$.

Hence we expect (for different reasons) that $\alpha = 3/2$ identically outside of the range of Fig. 24, for $n_1, n_2 \geq 0$. On the ordinate axis of Fig. 24, where $n_1 = 0$, we recover for meanders the announced transition at $n_2 = q = 2$, beyond which the DPL² model is no longer critical; numerical results however get poorer as we approach this point and we could not confidently analyze it numerically so far. In the case of semi-meanders, we have predicted an earlier “winding” transition point at $n_2 = q_c = 2 \cos \pi(\sqrt{97} - 1)/48$. More generally, the configuration exponent for multi-component and multi-river semi-meanders (one half-line plus an arbitrary number of river loops) is predicted to be

$$\begin{aligned} \bar{\alpha}(n_1, n_2) &= \alpha(n_1, n_2) - 1 + 2\Delta_1(n_1, n_2) \\ &= 1 + \frac{1}{24} \left(\sqrt{25 - c(n_1, n_2)} + \sqrt{1 - c(n_1, n_2)} \right) \sqrt{6(1 - e_1) - 4c(n_2)}, \end{aligned} \quad (5.3)$$

where $c(n_2) = 1 - 6e_2^2/(1 - e_2)$ and $n_i = 2 \cos \pi e_i$. The range of validity of (5.3) is smaller than the domain of Fig. 24, as it is delimited by the curve $3(1 - e_1)/2 + 6e_2^2/(1 - e_2) = 1$, with $n_i = 2 \cos \pi e_i$ (it is represented in dashed line on Fig. 24). The latter corresponds to a winding transition as explained above, where the number of pieces of road winding around the source of the semi-infinite river becomes relevant. Above that curve, we expect the semi-meander configuration exponent to identically vanish.

5.2. Extensions

Extending the generalization of the previous subsection, we could consider *both* complicated river geometries and keeping n_1, n_2 finite. This requires some care when dealing with the electromagnetic operators creating river vertices, as several geometries might correspond to the same correlators. Also extra care should be exercised when imposing that the meandric objects be *connected*: in the multi-river and multi-road case, a meander must be globally connected, but can have disconnected rivers or roads. We may also define higher-genus meandric numbers [5] which can also be enumerated by transfer matrix techniques, for instance on a torus.

As discussed before, we may also consider the coupling of the FPL² model to Eulerian gravity, namely by summing over genus zero tetravalent graphs with only faces of even valency. Then all the above predictions are expected to still hold, except that we must take the formula (2.3) for the central charge, that remains one unit above that of the DPL² model as we have ensured the vertex-bicolorability of the graphs we sum over [20]. Note that, in this Eulerian case, the b-vertex of Fig. 1 is now relevant and we *must* take $y \neq 0$ to get the above shifted central charge. The range of validity of Fig. 24 is reduced in this case to the zone of the square $[0, 2] \times [0, 2]$ delimited by the curve $c = 1$ joining the point $(2, q^*)$ to the point $(q^*, 2)$, with $q^* = 2 \cos(\pi(\sqrt{13} - 1)/6) = 0.410135 \dots$. One should also be able to check numerically the predictions for Eulerian gravity, using a suitable modification of our transfer matrix technique, in order to incorporate the vertex-bicolorability.

Another direction of generalization would be to consider more loop colors. For instance, one can define folding problems of two-dimensional lattices onto a d -dimensional target space, that in turn correspond to fully-packed loop models with a given number of loop colors, related to d . Attaching a different fugacity for loops of different colors, we may generate different universality classes, described by different conformal theories. Upon coupling to two-dimensional quantum gravity, these models would correspond to multi-colored meanders of some kind.

A final direction of generalization would be to add “matter” to the meandric graphs. Indeed, imagine we would like to consider a more involved model for a compactly folded polymer (protein), by attaching to its nodes a spin variable with inter and intra-chain Ising-like interactions. Then a simple way of describing it would be by first defining this matter spin model on the configurations of the square lattice fully-packed loop model, and then switching on gravity. If the matter model is still conformal, this should immediately lead to new configuration exponents for meanders in the presence of matter.

5.3. Algebraic exponents

It is both interesting and sad to notice that the only meandric numbers that can be calculated exactly with reasonably simple combinatorial formulas are all in one way or another related to Catalan numbers, and the corresponding exponents are always integers or half-integers (take for instance the case $n_1 = 0$, $n_2 = 1$, then $c = -2$, $\alpha = 3$, $\bar{\alpha} = 3/2$).

For general rational values of the e_i , we predict however that the exponents are algebraic numbers, roots of some quadratic equations with integer coefficients. Remarkably, such exponents are not commonplace in physics, but have emerged in some recent works on random walks [32,33]. If we could devise some relation between the meander problems and this other type of problems, we would probably be able to get a mathematically rigorous proof of our predictions.

Acknowledgements: We thank O. Golinelli for useful discussions.

References

- [1] A. Sainte-Laguë, *Avec des nombres et des lignes (Récréations mathématiques)*, Vuibert, Paris (1937).
- [2] K. Hoffman, K. Mehlhorn, P. Rosenstiehl and R. Tarjan, *Sorting Jordan sequences in linear time using level-linked search trees*, Information and Control **68** (1986) 170–184.
- [3] V. Arnold, *The branched covering of $CP_2 \rightarrow S_4$, hyperbolicity and projective topology*, Siberian Math. Jour. **29** (1988) 717–726.
- [4] K. H. Ko and L. Smolinsky, *A combinatorial matrix in 3-manifold theory*, Pacific. J. Math **149** (1991) 319–336.
- [5] P. Di Francesco, O. Golinelli and E. Guitter, *Meander, folding and arch statistics*, Mathl. Comput. Modelling **26** (1997) 97–147.
- [6] J. Touchard, *Contributions à l'étude du problème des timbres poste*, Canad. J. Math. **2** (1950) 385–398.
- [7] W. Lunnon, *A map-folding problem*, Math. of Computation **22** (1968) 193–199.
- [8] P. Di Francesco, O. Golinelli and E. Guitter, *Meanders: a direct enumeration approach*, Nucl. Phys. B **482** [FS] (1996) 497–535.
- [9] O. Golinelli, *A Monte-Carlo study of meanders*, preprint cond-mat/9906329, to appear in Eur. Phys. J. B (2000).
- [10] I. Jensen, *Enumerations of plane meanders*, preprint cond-mat/9910313 (1999).
- [11] E. Brézin, C. Itzykson, G. Parisi and J.-B. Zuber, *Planar diagrams*, Comm. Math. Phys. **59** (1978) 35–51.
- [12] S. Lando and A. Zvonkin, *Plane and projective meanders*, Theor. Comp. Science **117** (1993) 227–241; *Meanders*, Selecta Math. Sov. **11** (1992) 117–144.
- [13] Y. Makeenko *Strings, matrix models, and meanders*, Nucl. Phys. Proc. Suppl. **49** (1996) 226–237.
- [14] G. Semenoff and R. Szabo *Fermionic matrix models*, Int. J. Mod. Phys. A **12** (1997) 2135–2292.
- [15] L. Chekhov and C. Kristjansen, *Hermitian matrix model with plaquette interaction*, Nucl. Phys. B **479** (1996) 683–696.
- [16] B. Eynard and C. Kristjansen, *More on the exact solution of the $O(n)$ model on a random lattice and an investigation of the case $|n| > 2$* , Nucl. Phys. B **466** [FS] (1996) 463–487.
- [17] P. Di Francesco, O. Golinelli and E. Guitter, *Meanders: Exact asymptotics*, preprint cond-mat/9910453, to appear in Nucl. Phys. B (2000).
- [18] J. L. Jacobsen and J. Kondev, *Field theory of compact polymers on the square lattice*, Nucl. Phys. B **532** [FS], (1998) 635–688; *Transition from the compact to the dense phase of two-dimensional polymers*, J. Stat. Phys. **96**, (1999) 21–48.

- [19] V. G. Knizhnik, A. M. Polyakov and A. B. Zamolodchikov, *Fractal structure of 2D quantum gravity*, Mod. Phys. Lett. A **3** (1988) 819–826; F. David, *Conformal field theories coupled to 2D gravity in the conformal gauge*, Mod. Phys. Lett. A **3** (1988) 1651–1656; J. Distler and H. Kawai, *Conformal field theory and 2D quantum gravity*, Nucl. Phys. B **321** (1989) 509.
- [20] E. Guitter, C. Kristjansen and J. Nielsen, *Hamiltonian cycles on random Eulerian triangulations*, Nucl. Phys. B **546** [FS] (1999) 731–750; P. Di Francesco, E. Guitter and C. Kristjansen, *Fully packed $O(n=1)$ model on random Eulerian triangulations*, Nucl. Phys. B **549** [FS] (1999) 657–667.
- [21] P. Di Francesco, E. Guitter and J. L. Jacobsen, work in progress.
- [22] B. Eynard and C. Kristjansen, *An iterative solution of the three-colour problem on a random lattice*, Nucl. Phys. B **516** (1998) 529–542.
- [23] F. David and B. Duplantier, *Exact partition functions and correlation functions of multiple Hamiltonian walks on the Manhattan lattice*, J. Stat. Phys. **51**, (1988) 327–434. H. Saleur, J. Phys. A **19** (1986) L807–L810.
- [24] B. Nienhuis, in *Phase transitions and critical phenomena*, edited by C. Domb and J. L. Lebowitz (Academic, London, 1987), Vol. 11.
- [25] P. Di Francesco, H. Saleur and J.-B. Zuber, *Modular invariance in non-minimal two-dimensional conformal theories*, Nucl. Phys. B **285** (1987) 454–480.
- [26] H. Saleur, *Polymers and percolation in two dimensions and twisted $N=2$ supersymmetry*, Nucl. Phys. B **382** (1992) 486–531.
- [27] I. G. Enting, *Generating functions for enumerating self-avoiding rings on the square lattice*, J. Phys. A **13** (1980) 3713–3722.
- [28] B. Derrida, *Phenomenological renormalisation of the self avoiding walk in two dimensions*, J. Phys. A **14** (1981) L5–L9.
- [29] H. W. J. Blöte and M. P. Nightingale, *Critical behaviour of the two-dimensional Potts model with a continuous number of states: A finite size scaling analysis*, Physica A **112** (1982) 405–465.
- [30] P. Di Francesco, E. Guitter and C. Kristjansen, *Integrable 2D Lorentzian gravity and random walks*, preprint hep-th/9907084, to appear in Nucl. Phys. B (2000).
- [31] B. Durhuus, J. Frölich and T. Jónsson, Nucl. Phys. B **240** (1984) 453–480; F. David, Nucl. Phys. B **487** [FS] (1997) 633–649.
- [32] G. Lawler, O. Schramm and W. Werner, *Values of Brownian intersection exponents I: half plane exponents*, preprint math.PR/9911084 (1999).
- [33] D.S. Fisher, P. Le Doussal and C. Monthus, *Random walkers in 1-D random environments: Exact renormalization group analysis*, Phys. Rev. E **59** (1999) 4795–4840.